The ILIMA ring detector for particle identification, life time measurement and beam diagnostics

Technical Report for the Design, Construction and Commissioning of The Heavy Ion Detector

November 2, 2017

ILIMA	Name	E-Mail
Project Leader/Spokesperson	Takayuki Yamaguchi	yamaguti@mail.saitama-u.ac.jp
Deputy	Yuri Litvinov	Y.Litvinov@gsi.de
Technical Coordinator	Yuri Litvinov	Y.Litvinov@gsi.de
Project Manager	Helmut Weick	H.Weick@gsi.de
Contact Person at the FAIR site	Helmut Weick	H.Weick@gsi.de
Detector Convener	Roman Gernhäuser	Roman.Gernhaeuser@tum.de
Deputy	Thomas Faestermann	Thomas.Faestermann@ph.tum.de

The ILIMA Collaboration

Australia

Australian National University: Gregory Lane

Austria

Austrian Academy of Science: Paul Bühler, Johann Marton
IAEA Vienna: Milan Matos

Belgium

Université libre de Bruxelles: Stephane Goriely, Paul-Henri Heenen, Kohji Takahashi

Canada

TRIUMF: Iris Dillmann

China

Beihang University: Baohua Sun
Institute of Modern Physics, Chinese Academy of Sciences: Xiangcheng Chen, Xinwen Ma, Ruishi Mao, Zhiyu Sun, Xiaodong Tang, Xiaolin Tu, Meng Wang, J. X. Wu, Guoqing Xiao, Hushan Xu, Xinliang Yan, Zheng Yong, Youjin Yuan, YuHu Zhang, Liu Zhong, Xiaohong Zhou

France

Laboratoire Rene Bernas du CSNSM, Orsay: Georges Audi, David Lunney
CEA, IRFU: David Boutin

Germany

Facility for Antiproton and Ion Research: Alexander Herlert
GSI Helmholtzzentrum für Schwerionenforschung: Eugen Badura, Carsten Brandau, Timo Dickel, Christina Dimopoulou, Dmytro Dmitriev, Oleksiy Dolinskyy, Peter Egelhof, Bernhard Franczak, Bernhard Franzke, Hans Geissel, Frank Herfurth, Jan Hoffmann, H.-Jürgen Kluge, Ronja Knöbel, Christophor Kozhuharov, Ivan Kulikov, Nikolaus Kurz, Natalia Kuzminchuk, Sergey Litvinov, Yuri Litvinov, Gottfried Münzenberg, Frank Nickel, Chiara Nociforo, Fritz Nolden, Wolfgang Quint, Shahab Sanjari, Christoph Scheidenberger, Haik Simon, Ragandeep Singh, Markus Steck, Thomas Stöhlker, Gleb Vorobjev, Helmut Weick, Martin Winkler
Johannes-Gutenberg-Universität in Mainz: Karl-Ludwig Kratz, Bernd Pfeiffer
Johann Wolfgang Goethe-Universität Frankfurt: Rene Reifarth
Justus-Liebig-Universität Gießen: Ali Najafi, Wolfgang Plaß
Max-Planck-Institut für Kernphysik Heidelberg: Klaus Blaum, Sebastian George, Adriana Palffy
Technische Universität Darmstadt: Almudena Arcones, Achim Schwenk, Stefan Typel
Technische Universität München: Thomas Faestermann, Roman Gernhäuser, Gabriele-Elisabeth Körner, Peter Ring

Greece

Aristotle University of Thessaloniki: Georgios Lalazissis

Hungary

University of Zagreb: Dario Vretenar

India

University of Jammu, Rani Devi,

Italy

Laboratori Nazionali del Sud: Agatino Musumarra

Japan

Niigata University: Takashi Ohtsubo
RIKEN Nishina Center: Sarah Naimi, Tomohiro Uesaka
Tsukuba University: Akira Ozawa
Saitama University: Zhuang Ge, Takeshi Suzuki, Takayuki Yamaguchi

Poland

University of Warsaw: Zenon Janas, Zygmunt Patyk, Marek Pfutzner

Russia

NRC Kurchatov Institute: Ivan Borzov
St. Petersburg Nuclear Physics Institute: Yuri Gusev, Yuri Novikov
St. Petersburg State University: Sergey Torilov

Serbia

Vinča Institute of Nuclear Sciences: Dragan Toprek

Slovenia

J. Stefan Institute Ljubljana: Matej Lipoglavsek

Spain

Instituto de Estructura de la Materia (IEM-CSIC): Rayner Rodriguez-Guzman

Turkey

University of Istanbul: Rabia Cakirli

United Kingdom

University of Edinburgh: Philip Woods
University of Manchester: David Cullen
University of Surrey: Gavin Lotay, Zsolt Podolyak, Philip Walker

United States of America

Los Alamos National Laboratory: Dave Madland, Peter Moeller, David Vieira
Michigan State University: Marc Hausmann, Fernando Montes, Hendrik Schatz
Ohio University: Zach Meisel
Texas A&M University: Lixin Chen

Contents

Executive Summary **1**

1 Introduction **3**

2 Scientific requirements **6**
2.1 Conceptual Design 7
2.2 Combined detector concept 8

3 Detector and sensor units **9**
3.1 Pad detectors for energy loss measurement 10
3.2 Strip detectors for position measurement 10
3.3 Active stopper for the full energy measurement 11
3.4 Passive degrader 12

4 Electronics and Data Acquisition **13**
4.1 Overview and Concept 13
4.2 Analogue electronics 14
4.3 Digital electronics 15
4.4 Time stamping 15
4.5 Slow Control 16

5 Prototype experiment at the ESR **18**
5.1 Beam preparation and measurement cycles 18
5.2 Detector configuration 19
5.3 Energy resolution and particle identification 20
5.3.1 Beam Simulations 24

6 Mechanical Structure and detector position in the CR **27**
6.1 Mechanical Concept 27
6.2 Detector pocket for the CR 29
6.3 A compact detector module 30

7 Radiation Environment and Safety Issues **31**

8 Infrastructure **32**

9 Installation Procedure **33**

10 Time Schedule and Organisation **34**
10.1 Time schedule and Milestones 34
10.2 Organisation and responsibilities 35

11 Costs and Fundings **36**
11.1 Summary of the expected Costs 36
11.2 Funding scheme 36

References **39**

Executive Summary

The ILIMA (Isomeric states, Lifetimes, and Masses) project will focus on different aspects of nuclear physics using complementary techniques. Major highlights will be achieved by mapping of large areas of the unknown mass surface near and at the drip-lines, where loosely bound nucleons are interacting with the extremely asymmetric nuclear matter. Around the N = Z line the special shell configuration allows the investigation of the neutron-proton interaction which is of particular interest at the shell closures. Even more exotic nuclei at the pathways of nucleosynthesis in stars (r- and rp-process) will be studied to verify the influence of proposed waiting-point nuclei on the final solar abundances, as well as to explore the predicted shell quenching far from stability. For all these studies a precise measurement of the masses and lifetimes of highly-charged ions, their decay modes, and particle-emission branching ratios is the essential input required for astrophysical models. Additional contributions from isomeric states and their related nuclear properties will be determined by using pure isomeric beams.

In addition to the Schottky Mass Spectrometry (SMS) and the Isochronous Mass Spectrometry (IMS) methods a heavy-ion particle detector will be used for the ILIMA experiments. This detector will be a complementary tool serving several tasks at a time, e.g. for an independent half-life measurement, particle identification in mass and charge, and as additional beam diagnostics tool. It may also be used to detect and identify the heavy products of reactions in EXL-type experiments. The detector will be mounted in different pocket positions in the CR and the ESR . These pockets are equipped with a thin window made of typically 25μm stainless steel to separate the gas pressure inside the pocket from the ultrahigh vacuum (UHV) in the ring. Due to the massive changes in magnetic rigidity of even the heaviest ions by changing their nuclear charge in decay processes, daughter nuclei are typically well separated from their parent's trajectories at these points. This allows to insert an active stopper for the reaction products while the beam in the ring will not be affected and non-destructive mass measurements via SMS can run in parallel. Half-lives of the detected nuclei will be deduced from the rates of impinging daughter nuclei while the orbiting parent nuclei are continuously monitored by the Schottky pickups.

The heavy ion detector will be essentially unique for exotic decay modes like the β-delayed neutron emission which will be the dominant decay channel for the most exotic nuclei on the r-process path or even beyond. The same holds for α-decays. In all of these cases the reaction products will end up outside of the acceptance of the ring but their trajectories still reach the plane of the heavy ion detector.

In case of bound-state β-decay at very low Q-values this detector will be also extremely advantageous. While the decay products undergo only a minimum change in mass they are collected over long periods in the ring. When switching on a gas stripper, they will lose an additional electron within a few revolutions and change immediately their mass-to-charge ratio and are collected in the heavy ion detector. Due to the active electron and stochastic cooling this process could be repeated several times to directly deduce the corresponding half-lives.

One of the important systematic contributions in the SMS measurements is a precise determination of beam-loss processes during the storage. Electron pickup in the cooler or the rest gas are non-negligible effects independently determined by the heavy ion detector through its particle identification. As particles with a charge (q−1) also significantly change their trajectories, they will be also collected in the detector but separated according to their position and energy-loss pattern from the reaction products. A direct comparison between ion-optical calculations and the measured particle distributions in all these different cases may be used especially in the commissioning phase of the CR for an improved understanding of the machine using full ion optical simulations.

This document is the result of an extensive R&D program performed over the last years. It presents the technical choices for the heavy ion detector CsISiPHOS (CsI-Silicon Particle detector for Heavy ions Orbiting in Storage rings) for the ESR and a slightly modified version for the CR. The design and the inherent details associated with its construction are illustrated in this TDR. It should be noted that the CsISiPHOS-type heavy ion detector will itself be an independent device that can be adapted for use in experiments as a standalone detector.

1 Introduction

The detectors for the ILIMA experiment will be installed at the Collector Ring after the Super-**FR**agment-**S**eparator 'Super-FRS' at FAIR, the **F**acility for **A**nti-proton and **I**on **R**esearch, and will allow a wide experimental program on short lived radioactive nuclei.

The ILIMA activity is a major branch of the NUSTAR (**NU**clear **ST**ructure, **A**strophysics and **R**eactions) pillar of the FAIR experimental program.

The ILIMA [WLG13] experimental program is based on the combination of the in-flight separator Super-FRS and a system of storage rings. The Super-FRS will be an ideal tool to provide short-lived nuclides of all elements lighter than uranium for precise mass- and half-life measurements in the new storage rings. Unique investigations of decay modes and half-lives of stored highly-charged nuclides are possible, as well as access to pure isomeric beams.

Two methods have been developed for precise mass measurements of stored exotic nuclei: The 'Schottky Mass Spectrometry (SMS)' for electron-cooled beams of longer-lived isotopes with $t_{1/2}$>1 s, and the 'Isochronous Mass Spectrometry (IMS)' for short-lived fragments with half-lives down to $t_{1/2}\approx 10$ μs. Both methods, well established in previous experiments, are based on precise measurements of the revolution frequency which unambiguously characterizes the mass-to-charge ratio of the circulating ions, either with Schottky pickups (SMS) or with time-of-flight detectors inside an isochronically tuned storage ring (IMS). A great advantage of both, SMS and IMS is that the mass of a single ion circulating in the ring can be measured. These two experimental methods are especially well-suited to measure effectively a large part of the mass surface in one run. In this way the systematic errors can be kept small if the reference masses for the calibration are known well enough.

The lifetimes of stored nuclei can be obtained with two independent methods. The first one is to measure directly the intensity changes of the stored ion beams. The second is based on the fact that daughter and parent nuclei differ by their mass-to- (nuclear) charge ratio. Then the decay to the resulting daughter nuclei can be recorded with particle detectors placed near the orbit of parent nuclei circulating for several half-lives in the ring. Both methods yield redundant information by simultaneous measurement of the decay of the parent and the population of daughter nuclides.

Today the challenge is to measure the masses and the lifetimes of exotic nuclides up to the limits of nuclear existence. In this way the location of the drip-lines can be experimentally determined and the new properties of very exotic nuclides can be investigated for the first time.

Nuclei in isomeric states were already observed throughout the campaign for mass and life-time measurements with the present FRS-ESR facility. Depending on the half-life and excitation energy of isomeric states a pure isomeric beam can be prepared. The existing FRS-ESR facilities are used to develop the experimental methods proposed for ILIMA.

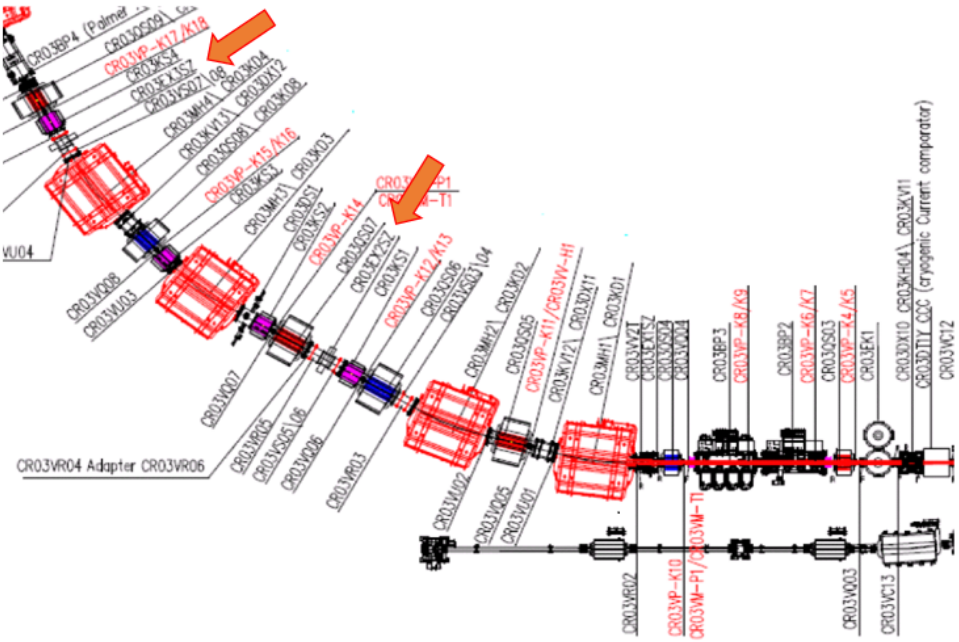

Figure 1.1: *The north-east arc of the Collector Ring with two out of four detector positions at CR03EX2SZ, and CR03EX3SZ (beam from the right). Two further optional positions are foreseen on the opposite side of the ring at CR01EX3SZ and CR01EX4SZ. Each position can be equipped with two movable pockets for heavy ion detectors either from inside the arc or from its outer side.*

The improved performance of the upcoming detector systems will already be used in the Phase 0 campaign proposed for the years 2018 - 2022.

The design and construction of the detector is being pursued within the ILIMA collaboration, a large international consortium comprising more than 110 scientists from 20 countries. The relevant physics cases and detailed conceptual layout of the project including its instrumental parts have been laid out in the Conceptual Design Report for FAIR [Gut01] in 2001 and at a more in-depth level in the ILIMA Technical Proposal [WL06] in 2006.

In an extensive R&D program the heavy ion detector CsISiPHOS (CsI-Silicon Particle detector for Heavy ions Orbiting in Storage rings) was developed, and its great performance was demonstrated. While the details on its design are shown in chapter 3 the results of a full-scale experiment are discussed in chapter 5.

In chapter 2, we outline the different working modes for the heavy ion detectors implemented at eight optional positions (see figure 1.1) and a selection of particular physics cases for which the detector with its demanding requirements will play an important role.

The front-end electronics (FEE) and data acquisition (DAQ), summarized in chapter 4, are designed mainly within the NUSTAR Synergy Group for Front-End-Electronics and Data Acquisition (SGFD), in close coordination with the ILIMA working group. The mechanical support presented in chapter 6 follows the idea of a digitally-controlled UHV pocket similar to the detector pockets used currently in the ESR. Different radiation and safety issues are discussed in chapter 7, whereas plans on specific infrastructure related issues and the detector installation procedure in its final location are presented in chapters 8 and 9 respectively.

The expected time schedule in the construction and installation is described in detail in the working plan presented in chapter 10. Explicit financial evaluation of the cost related to this detector, together with the collaboration engagement is presented in chapter 11.

2 Scientific requirements

Nuclear masses and lifetimes of exotic nuclei in ground and isomeric states are basic quantities which are essential for the understanding of nuclear structure and the creation of the elements in stars. Today the challenge is to measure the masses and lifetimes of exotic nuclei up to the limits of nuclear existence. From systematic precision measurements with the variation of neutron (proton) number along isotopic (isotonic) chains important information can be derived, like the location of the drip-lines, the development of shell closures, the changes in shapes, and pairing. New experimental developments involving storage rings yield access to measurements of bare and few-electron ions in the laboratory, thus under conditions that prevail in hot stellar environments. A great research potential is offered by the fact that not only ground-state properties can be studied but also those of isomeric states, which are populated in projectile fragmentation and fission at relativistic energies.

The experimental possibilities will expand with the availability of pure isomeric beams that can be used for secondary nuclear reactions, which will open novel ways to explore the nuclear structure.

Storage-ring based decay spectrometry has proven to be an extremely effective and sensitive technique for addressing basic nuclear properties like binding energies, lifetimes and branching ratios in exotic nuclei. The β-decay experiments of highly-charged ions at the experimental storage ring (ESR) at GSI Darmstadt have been a rich source of new discoveries about decay properties of nuclei [LB11, BLS13]. The exciting discovery of the bound-state β^- decay in 1992 [JBB$^+$92, BFF$^+$96], the discovery of new isotopes and accurate measurements of their masses with Schottky and isochronous mass spectrometry [CPG$^+$10, SCL$^+$13], and finding new long-lived K-isomers [DWK16, RCW$^+$10] are a few examples of the accomplishments from the FRS-ESR facility. Owing to this success, the ILIMA (Isomeric states, Lifetimes, and Masses) Collaboration has been founded at FAIR. Within the MSV, ILIMA aims principally at performing experiments in the Collector Ring (CR) and the Experimental Storage Ring (ESR) but also makes use of the HESR and the Cryring.

The required experimental capabilities are unique to GSI-FAIR, firstly in the sense that fully-stripped high-Z ions can only be produced and separated with projectiles at energies around 1 AGeV, and secondly because a significant fraction of the elements are refractory and particularly difficult to study with ISOL techniques.

In a typical ILIMA experiment the radioactive ions pre-separated in the FRS/SuperFRS are injected into the ESR/CR where the high mass-resolving power of a few hundred thousand allows for the direct resolution of ion species with different mass-to-charge ratios by their revolution frequencies. Schottky pickups enable single-ion identification with mass/energy uncertainties down to 10−100 keV.

Direct particle detection of reaction products is a complementary experimental method that is unique in certain applications. Especially in case of β-delayed one- and two-neutron

emission the daughter nuclei may not be stored on stable trajectories in the ring and have to be detected shortly after the decay. Measuring single ions right after their decay also allows for a cross calibration of the Schottky power spectra to fully control systematic uncertainties. Also the losses of highly charged ions due to electron pickup in the cooler (ESR, HESR) can be determined independently. As an additional contribution a position sensitive measurement of the decay products allows to adjust the ring parameters "online".

2.1 Conceptual Design

A multi-purpose particle detector will be a key device in the ILIMA program [WL06] in the future CR [Gut01] [Nov16]. Already now it is foreseen to be used in the FAIR Phase-0 experiments at the ESR. This detector will be a complementary tool serving several tasks at a time for an independent half-life measurement, particle identification in mass and charge, and beam diagnostics. It may also be used to detect and identify the heavy products of reactions in EXL-type experiments.

Experiments at large scale storage rings provide a set of significant experimental challenges and typically do not allow for a direct identification of the stored beam particles without immediately destroying the beam quality. Also a direct insertion of detector elements and their corresponding mounting structures, cabling and vacuum ports into the ultra high vacuum (UHV) of about 10^{-11} mbar of a storage ring affects the quality parameters of the device. In addition the UHV constraints and typical mounting cycles strongly limit flexibility of such a device that has to be optimized for individual experiments.

An efficient solution is provided by the concept of movable detector pockets inserted at different points into the ring. These pockets are equipped with thin windows made of typically 25μm stainless steel to separate the gas pressure inside the pocket from the UHV in the ring. During the filling cycle these pockets are moved to a parking position outside the acceptance of the ring. In the CR, after the bunch rotation and stochastic cooling with small beam envelopes they are quickly inserted to their measurement position close to the narrow beam trajectory. It is important that the detectors are placed at positions with enough dispersion to separate circulating beam and ions which e.g. have changed their charge after β decay. On the way to the detector the dispersion must also not be larger, otherwise poor transmission at the detector is the result. Calculations for the CR have shown that a position after the first two dipoles following the straight sections of the ring are well suited for detection of charge change in the region around Z=50, and after four dipoles for Z around 82. The beam positions and widths can be calculated from the optics parameters of the CR as shown in Figure 2.1.

Due to the massive changes in magnetic rigidity of even the heaviest ions changing their nuclear charge in β-decay processes, electron pick-up or particle emission, daughter nuclei are typically well separated from their parents trajectories at these points. This allows to insert an active stopper for the reaction products while the beam in the ring will not be affected and (non-destructive) mass measurements via SMS can run in parallel. Half-lives of the nuclei will be deduced from the rates of impinging daughter nuclei while the parent nuclei are continuously monitored by the SMS.

The observation of neutron emission delayed by preceding β-decay is one of the key cases. A decay can happen anywhere in the ring (due to the MHz orbiting frequency), but ions

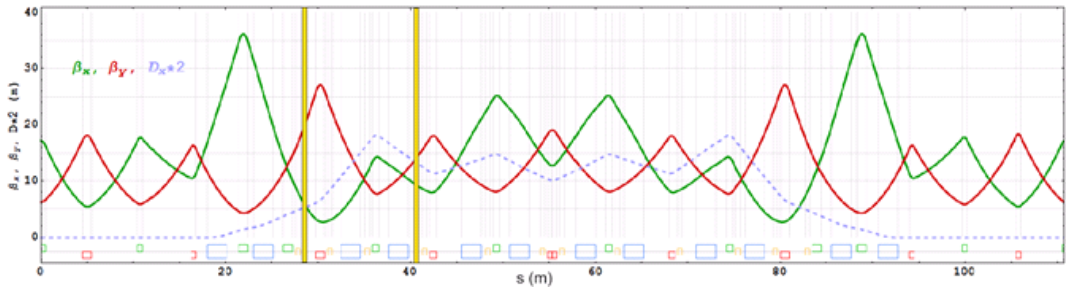

Figure 2.1: Beta and dispersion functions in RIB mode of CR, from the CR-TDR Annex1 [Nov16] (Fig.2.5-10). The positions for detector pockets are indicated by the yellow lines. They are close to horizonthal waists and at moderate or high dispersion respectively.

changing charge in the straight sections will all follow the same dispersion curve and can be efficiently collected on a detector in the arc. A test for this detection method was done in the ESR, and showed the ions located in a narrow peak (see chapter 5).

Based on its versatile applications a prototype design for the heavy-ion detector has been developed, implemented, and tested at the existing ESR facility. The basis for this design were earlier detector systems built by L. Maier et al. [Mai07] [MFK+01].

The detector has to provide a position resolution corresonding to the size of the source (the beam diameter) in the ring after cooling. In addition, the device must provide unique particle identification (PID) in mass and nuclear charge Z to allow a clear separation of isobaric contaminants. As the nuclei of interest have typical decay times of more than a second the rate capability, time resolution, and the dead time constraints are less crucial requirements. Major constraints are defined by the pocket geometry, the fast insertion of the pockets to the measurement position and the required resolution.

All these arguments led to the CsISiPHOS detector design.

2.2 Combined detector concept

CsISiPHOS is a heavy-ion telescope detector using a stack of five large-area single-sided silicon detectors (SSSDs) for a high resolution energy loss measurement, a massive CsI(Tl) detector to stop the particles and reconstruct their full energy complemented by a double sided silicon strip detector (DSSD) for the positions determination of each particle. All details on the layout, the mechanical implementation and the readout concept are discussed in the following two chapters.

3 Detector and sensor units

The detector concept of CsISiPHOS is based on a combined high-resolution measurement of several coincident observables. The multi-sampling energy-loss measurement allows for a clear separation of different nuclear charges. In combination with a total energy measurement a unique particle identification is achieved. An additional two-dimensional measurement of the impact position of heavy ions on the detector plane contains information on the magnetic rigidity of the particles, their charge state and also their decay vertex along the circumference of the ring. The combination of all these data provides an absolute measurement of decay properties of even the shortest-lived radioactive beams, and a strong reduction of background effects from beam contaminants.

The detector concept and its complexity does not allow for a direct implementation into the UHV of the ring. A very compact pocket structure is used to insert CsISiPHOS close to the beam trajectory in the ring vacuum while leaving the detectors themselves in a closed volume flushed with dry nitrogen. The detector array is designed in a modular way to allow for an easy exchange and precise positioning of the individual elements in a common housing (see figure 3.1) and therefore a perfect adaptation to the different measurement tasks. For this reason all elements are mounted on identical support frames which can be inserted into their main frame in eleven slots along the stack.

Unified connectors and a passive interface board are used to provide a compact cable interface to the singly shielded cables for the analogue signal transport. Here 0.50 mm so-called "Q-Strip" mini-ribbon high-speed coax cable assemblies from Samtec (HQCD-030-23.62-SED-SBR-1-N) showed a very good performance and reliability.

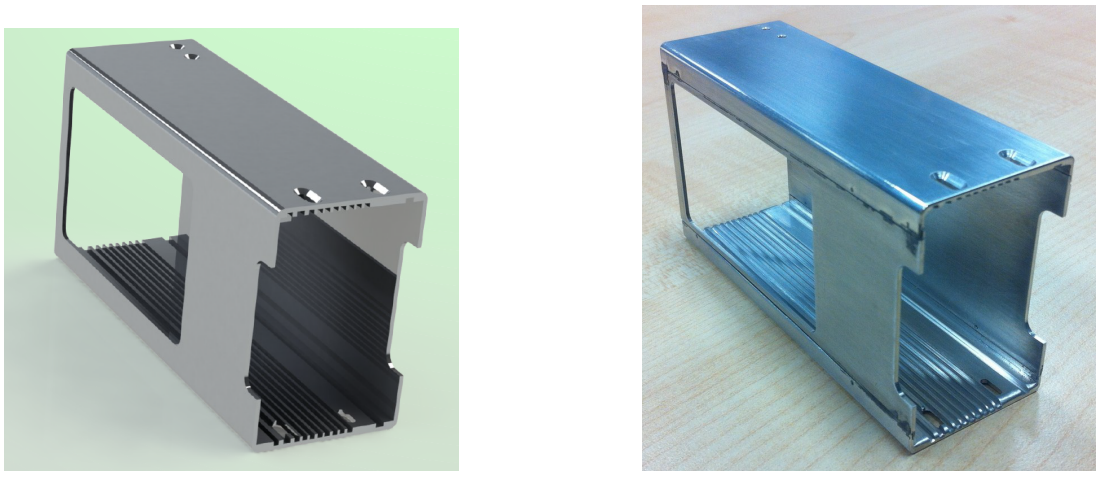

Figure 3.1: Left: CAD animation of the detector housing with eleven slots to insert different detector units. The entrance window has the dimensions 65×40 mm^2. Right: CsISiPHOS housing as used in the experiment discussed in chapter 5.

In the following sections the individual components of the detector as well as their technical specifications are described in detail.

3.1 Pad detectors for energy loss measurement

The first task of CsISiPHOS is to identify the nuclear charge of the reaction products impinging on the detector. This is done with single-sided silicon strip detectors (SSSDs) based on the 'Design I' chip by Micron Semiconductor Ltd, England for an active area of 60x40 mm^2. The 'design I' shows seven individual pads on the p-side, and its metallization has a grid structure (9G) with a thickness of 0.05 μm covering less than 2% of the active area. The n-side is fully metallized with a layer of aluminum and a thickness of 0.5 μm. These detectors are available at thicknesses of 300, 500, and 1000 μm. Balancing the requirements for energy resolution and efficiency this design was chosen. On one side the low segmentation reduces the number of inter-strip events which have to be suppressed in the later correlation analysis, while the limited area of each pad reduces the noise contributions from leakage current and detector capacity. To optimize in addition the multisampling capability a detector thickness of 500 μm turned out to be the best solution for the heaviest ions while 1 mm thick detectors may be chosen for the lighter ones. Fig 3.2 shows a sample of the pad detectors mounted on its corresponding PCB frame.

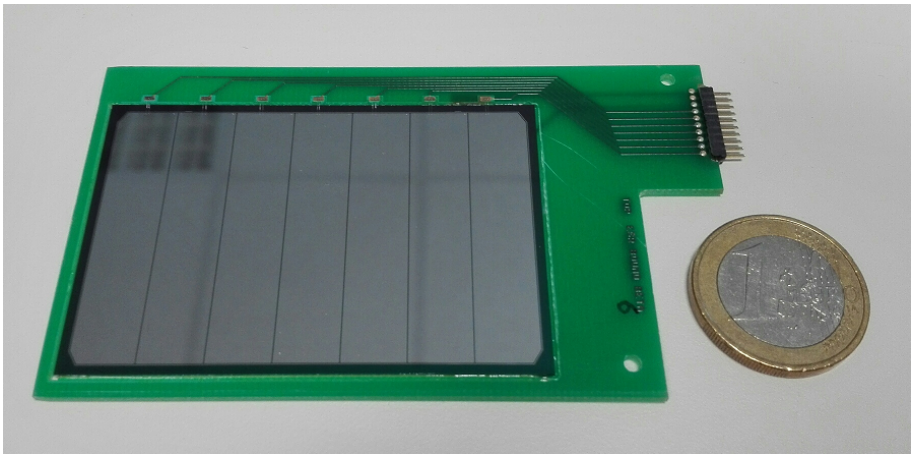

Figure 3.2: Layout of the pad detectors on their PCB. The seven strips are individually connected to the interface board while the unsegmented backside of the detector is connected to ground.

3.2 Strip detectors for position measurement

For the determination of the two-dimensional impact coordinates of each particle in the detector plane double-sided silicon strip detectors (DSSDs) are used. To minimize the number of analogue cables inside the detector pocket, a single resistive readout chain is used on each side of the detector to determine positions with a single strip resolution. The DSSDs are manufactured by Canberra Inc, USA (PF-60CT-40CD-60*40-300) and show a granularity of 60 vertical strips on the p-side and 40 horizontal strips on the n-side equally distributed over the active area of 60x40 mm^2. The resistive chain is built from

individual SMD (Surface mount device) resistors (size 0402) to form a total resistance of 3 kΩ between the two sides of a chain. While larger resistors would reduce the electronics noise they would on the other hand introduce a position dependent variation of the signal rise time. Experimental tests have shown that already an energy deposition of 20 MeV in a single strip of the detector allows for a 3 σ separation of the individual strips using this chain and standard analogue electronics.

Fig 3.3 shows a DSSD mounted on its corresponding PCB frame.

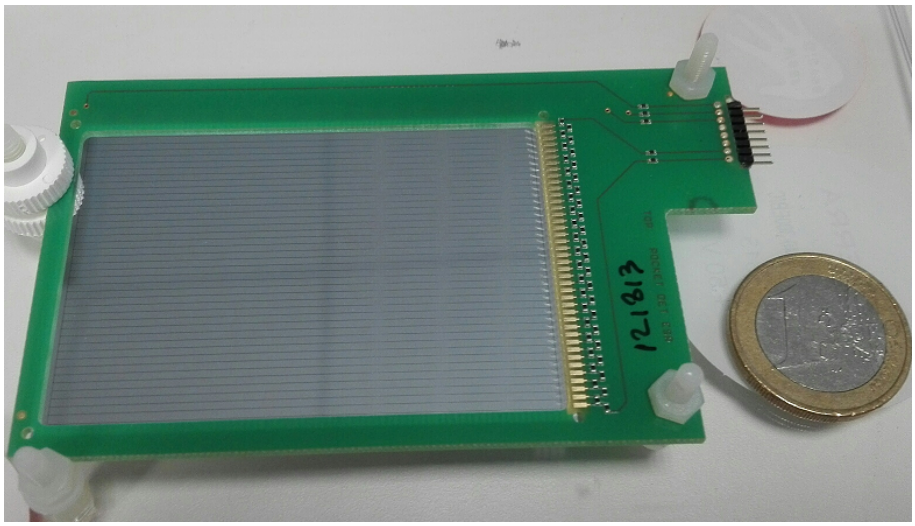

Figure 3.3: Photo of the DSSD's y-sensitive side on its PCB. The forty strips are connected to a resistive chain on the interface board.

3.3 Active stopper for the full energy measurement

For the mass identification of the particles their total energy is also determined. After electron cooling of the injected ions, the velocity of the particles inside the ring is very well defined with a precision of $\Delta\beta/\beta < 10^{-4}$. Here the total energy is directly related to the particle mass and should be determined with a precision of $\Delta E/E < 1/A$, while the energy loss in a rather thin layer of silicon determines the nuclear charge. This situation is different in an isochronous setting of the ring. In this case the detector has to provide unique particle identification without additional constraints. While the individual energy-loss measurements are altered by straggling in the material, the particles have to be stopped in the active material for such a high-resolution measurement. Taking into account the limited space in beam direction, a high-density scintillation material which could be easily operated in air was chosen as an active stopper. CsI(Tl) has a density of 4.51 g/cm^3, provides a very good light output in the visible range and is only very slightly hygroscopic. The peak wavelength of 455 nm nicely fits the sensitivity curve of regular silicon photodiodes. For the prototype experiment discussed in chapter 5 a 24x24 mm^2 large and 10 mm thick slice of CsI(Tl) was directly attached with optical cement (BC-600 by Saint Gobain Crystals, France) to a MSD35 chip from Micron semiconductor Ltd, England. The five open sides of the crystal were covered by highly reflective foil VM2000 (Vikuiti Projection Film manufactured by 3M, USA) to provide a homogeneous light collection over the full area.

3.4 Passive degrader

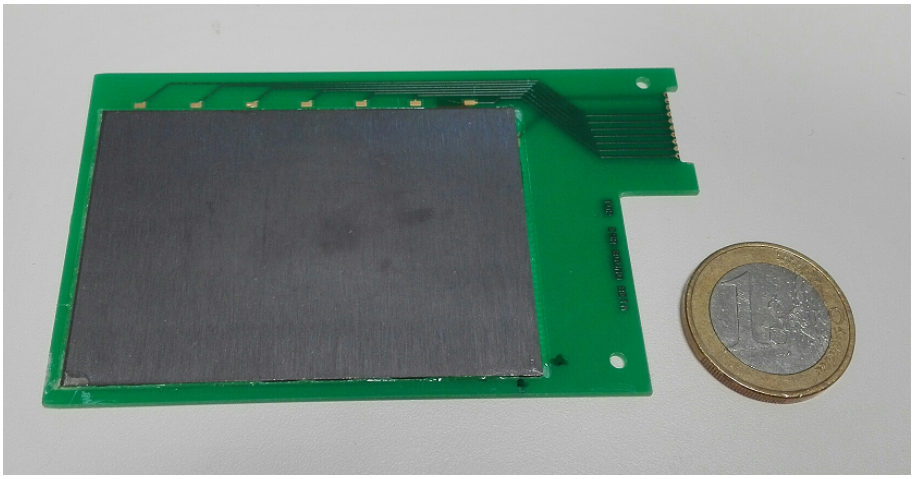

Figure 3.4: Photo of the 1 mm thick tantalum degrader. As it is mounted on a standard frame of the pad detectors it can be used in any slot of the detector stack.

A strong variation of the energy loss of different ion species and the limited space inside the detector pocket in some cases require even more dense stopping materials. For these cases one slot in the CsISiPHOS array between the energy-loss measurement and the active stopper is reserved to insert different passive degraders into the particles' trajectory. Tantalum with a density of 16.4 g/cm^3 has shown very good properties in this case. Similar to the detector mountings a slice of 60x40 mm^2 tantalum may be mounted on one of the detector frames which allow for a maximum thickness of 2 mm. Alternatively higher density scintillators like BGO (Bismuth Germanate, $Bi_4Ge_3O_{12}$, ρ= 7.13 g/cm^3) may be chosen in special cases for the active stopper. Here the modular concept of CsISiPHOS allows for significant variations without changing the readout and mechanics environment.

4 Electronics and Data Acquisition

Modern techniques of digital data acquisition have been found to be a major step forward in the next generation of detectors for nuclear physics. Especially the use of digital pulse-shape analysis provides unique features to reduce background and reduce ambiguities in the event pattern. While the current implementation of the readout electronics used for the prototype experiment at the ESR (see chapter 5) was based on classical shaping amplifiers, the new readout system for the heavy ion detector at the CR will build on the new developments of the NUSTAR DAQ group. It is of utmost importance for small systems like the pocket detector described here to minimize the maintenance effort and get the maximum support from the host facility.

While the old CsISiPHOS system will be used for all Phase-0 experiments at the ESR, the digital part will be completely renewed for the installation at the CR. This allows for a standard integration of a trigger-less system fully integrated into the White Rabbit time-stamping system developed for NUSTAR which can be combined with any other detector system at FAIR and the accelerator control itself. A fully digital data acquisition will in addition improve the the detector system significantly. Crosstalk and transient signals on the segmented silicon detectors will be recorded and allow for a separation of particles hitting the detectors close to the segmentation lines. The pulse-shape analysis of the light curves from the active stopper will give a clear separation of signals from fully stopped ions and those originating from nuclear reactions in the material. This effect is discussed in detail in the TDR for the CALIFA spectrometer of R3B [CAL14]. Especially searching for rare decay channels this improvement in signal-to-background ratio will be of utmost importance.

4.1 Overview and Concept

Heavy ions which are stopped in the detector stack as discussed in chapter 3 typically produce large signal amplitudes in all mounted silicon sensors. Therefore it is possible to route all signals out of the tight pocket geometry over 50 cm by special mini-ribbon high-speed coax cable assemblies (see section 3) without significant concessions on the signal-to-noise ratio. This allows to mount all the electronics components outside the gas volume of the pocket with rather relaxed space constraints. Here high resolution preamplifiers can be mounted on a massive platform electrically separated from the accelerator ground potential. Analogue charge-sensitive devices integrate the detector signals and transform them to differential current signals which can be transported over several meters of twisted pair cables to the digitizer modules. FEBEX3B digitizers, readout logic and the data acquisition PC with its White Rabbit interface sit in a rack close to the detector inside the cave just connected by glass fibers to the outside world. Taking into account the large scale of the new facility and the gigantic radiation shielding as well as the fact that this detector will be used at different locations along the CR or even in the ESR, this modular distributed concept minimizes the local infrastructure and the total overhead for

installation and maintenance. Just power, a TCP/IP and a clock interface are needed to operate the full system.

4.2 Analogue electronics

For the analog signal processing a standard set of amplifier modules from Mesytec[1] are implemented. This type of modules are been used in a large number of experiments at GSI, RIKEN or CERN and have several useful features. Already the standard version of the MPR-32 preamplifier[2] is dual gain with typically a factor of ten between the two settings to cover a wide range of heavy ions traversing the same detector. They can operate also large detector elements with an intrinsic capacity of up to 1 μF. Sixteen independent channels on a single board also nicely fit to the 16 channel digital layout discussed later. With a large open loop gain also the huge amount of charge from the heavy ion signals can be extracted very fast. In the CsISiPHOS configuration the p-sides of up to eight seven-fold segmented detectors for the energy loss are connected to two MPR-32 packages leaving channels 8 and 16 free for calibrations.

The backside of each detector is connected to one channel of an MSI-8 module[3], for trigger generation and redundant energy measurement in case of inter-strip events. Here individual high voltage connections for each detector from MHV-4 high voltage NIM modules[4] allow for an optimized depletion setting and individual monitoring of the leakage current for each detector in the CsISiPHOS stack. Also the four ends of the resistive chain of the DSSD and the p-side of the photodiode for reading out the CsI(Tl) detector are fed into one MSI-8 module which provides even more flexibility in the gain setting.

While the MSI-8 modules already have a built-in shaping amplifier as well as a timing filter stage with individual threshold settings, the signals of the MPR-32 modules go into four 16-channel shaping amplifiers STM-16+[5].

All modules provide again a large variety of gain settings and two different shaping times of 1−2 μs. Here individual channel thresholds are set by slow control to provide a channel and multiplicity trigger in the CsISiPHOS configuration for triggering the peak-sensing ADC MADC-32[6].

In the new configuration most of the latter modules are not needed any more. Just the output signals of the MPR-32 preamplifiers will be fed into four new FEBEX3B modules and all the signal processing will be done in a digital way as discussed in section 4.3. The preamplifier output from the two MSI-8 modules are fed into a fifth FEBEX3B module.

[1] http://www.mesytec.com/products/nuclear-physics.html
[2] http://www.mesytec.com/products/datasheets/MPR-16.pdf
[3] http://www.mesytec.com/products/nuclear-physics/MSI-8.html
[4] http://www.mesytec.com/products/nuclear-physics/MHV-4.html
[5] http://www.mesytec.com/products/datasheets/STM-16+.pdf
[6] http://www.mesytec.com/products/datasheets/MADC-32.pdf

4.3 Digital electronics

The FEBEX3B[7] (Front End Board with optical link EXtension, revision 3B, see figure 4.1) is a compact digitizer board including 16 fast sampling ADC channels (2x AD9252) sampling the input signal with up to 50 MS/s and a resolution of 14 bit. The ADC data streams are sent to the on-board FPGA (Lattice ECP3 150) for processing. Besides 150k LUTs, sufficient for very sophisticated firmware implementations, the FPGA features (among others) dedicated hardware multipliers, memory cells and various built-in high-speed I/O standards, which makes it perfectly suited for digital signal processing. Auxiliary electronics may be plugged on the FEBEX3B via a high-density extension connector carrying the 16 differential, analog inputs to the ADC channels and 16 general purpose LVDS I/Os (which can also be used as 32 single ended CMOS I/Os). Via a PCIe like connector, up to 19 FEBEX3B boards are plugged into one 19 inch crate for rack mounting. The FEBEX boards within a crate are daisy-chained using a bi-directional 1.6 Gbps connection for readout and control via the GOSIP protocol (Gigabit Optical Serial Interface Protocol) [MHKO10]. In addition, an 8-line MLVDS bus connecting all modules, is provided for trigger signal exchange (local triggerbus). The crates first slot (uplink) is equipped with a passive adapter board. It connects the GOSIP uplink of the first FEBEX module to the PEXOR[7] module inside the acquisition PC via an optical fiber. The PEXOR has four optical fiber connectors which enables the parallel readout of four FEBEX crates. Large on-board memory buffers ensure sufficient temporary event storage capacity for the subsequent DMA transfer to the PC memory via PCIe with a net speed of up to 600 MB/s. Using the same adapter, the MLVDS bus is connected to the EXPLODER[7] via a fine pitch flat ribbon cable.

The EXPLODER is a trigger logic box featuring a Xilinx FPGA, 8 NIM/TTL Lemo inputs, 8 NIM/TTL Lemo outputs, 2 local trigger bus connectors for up to four FEBEX crates, 8 differential ECL/LVDS inputs, 8 differential ECL outputs, 8 dfferential LVDS outputs and 4 optical fiber connectors. It is used for common dead-time blocking, complex trigger logics and interfacing external devices. Essential is the built-in USB plug which allows runtime configuration of the trigger logic. Via the ECL inputs and outputs it is connected to TRIXOR[7], the MBS trigger master, a PCIe board within the acquisition PC. An accepted readout trigger signal from any source arriving at the EXPLODER will be distributed to the TRIXOR and FEBEX boards. While the FEBEX boards are preparing the data to be sent to the PC, TRIXOR issues an interrupt request (IRQ) to the MBS software, which controls the readout. MBS causes PEXOR to send a digital token to the first FEBEX module of each GOSIP chain. After receiving the token, the FEBEX modules send the collected data upstream (i.e. to PEXOR via all FEBEX modules in between). Afterwards, the token is sent downstream to the next FEBEX module. After reading the last FEBEX module, the token returns to PEXOR to indicate the complete readout. MBS collects the received data and provides a network data stream for online monitoring and disk storage.

4.4 Time stamping

To allow for a general implementation of the detector system into any NUSTAR data acquisition system, a global time stamping based on the White Rabbit protocol [KAMF+14] will be used. This is distributed through an optical fiber to the MBS PCs using a PEXARIA[7]

[7] https://www.gsi.de/en/work/research/experiment_electronics/digital_electronic/digital_electronics/modules.htm

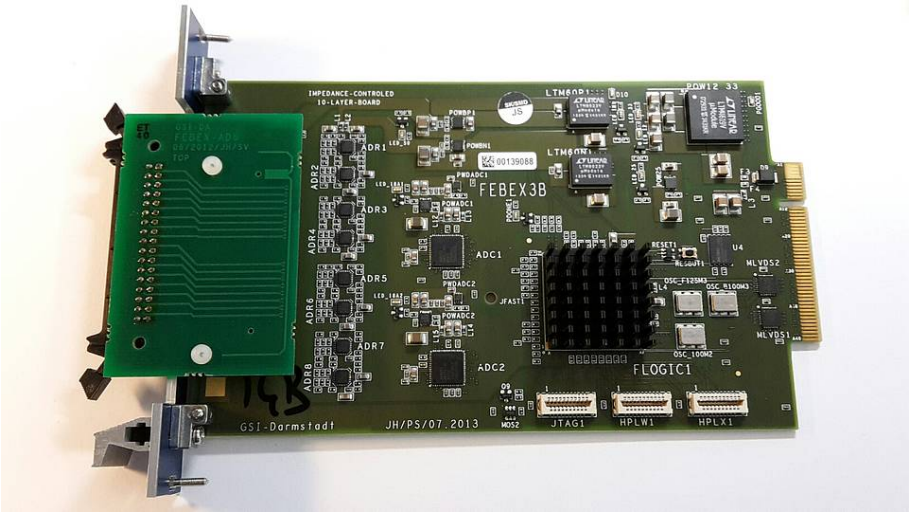

Figure 4.1: Photo of FEBEX3B card (taken from https://140.181.3.31/en/work/research/experiment_electronics/digital_electronic/digital_electronics/modules/lwl/febex/febex3b.htm).

card. The current time stamp is appended to the detector data before it is sent to a so-called time-sorter. The time-sorter receives the data from all sub-detectors (in this case just one) and stores it ordered by the time stamp. Assembly of physics events from the sub-detectors (in case of auxiliary devices to be implemented) will be done offline. Whenever a readout is triggered, a signal is also sent to the coaxial input of the PEXARIA cards, which causes the card to latch the current time stamp. Later, after the GOSIP readout is completed, that time stamp information is read from the PEXARIA card and appended.

As the detector will feature a free-running multi-event readout, and because the White Rabbit time stamps can only be used globally, an additional local time stamp for each individual hit is needed. To that end, the EXPLODER runs a local clock, which is propagated through the PCIe back-end to all the FEBEX modules. From this received clock, a 60 MHz clock is generated on the FPGA and each received event is marked with a local time stamp synchronized to that local clock. That way, the events on disk will be marked by a global time stamp, and the sub-events are marked with individual local time stamps. This allows for a redundant time reconstruction and a simplified event building.

4.5 Slow Control

During operation, all parts of the detector setup need to be configured and constantly monitored. This includes the preamplifier modules, bias voltages, leakage currents, the trigger conditions and the FEBEX firmware operation modes, shaping times, offset settings and data parameters but also the hardware settings like the positioning of the detector pocket within the beam line. The operation of the data acquisition must not be disturbed by any slow control action.

To be able to control and monitor the running system, and to correlate the accelerator status with the measurement without using a complicated database interface, slow control

events also marked with a unique White Rabbit time stamp will be merged into the MBS data stream, do be directly available by the latter analysis.

One special MBS trigger type is foreseen to activate a FEBEX add-on (C3PO) developed for tail pulse generation. This module is connected to all preamplifiers and will allow for a continuous monitoring of the gain stability and dead time of the full electronics chain. Another trigger will be used to write new parameter settings to the digital electronics and generate a slow control event with all parameter settings on-the-fly.

Both triggers are generated by software and injected into the Master Trigger Logic. In contrast to the usual readout triggers, those trigger signals are not distributed to the FEBEX modules but only to the f_user part of MBS which handles the request.

For *Control Triggers*, the new parameters are read from configuration files and stored to the electronics. A *Slow Control Event* containing a binary copy of the parameters is sent to the MBS Event Builder for later reconstruction of the detector state at any time. *Monitor Triggers* cause MBS to read the parameters from the modules, which will again be packed to a *Slow Control Event*.

For the control of external hardware and the accelerator interface one additional FEBEX module with its 16 digital I/O channels is used. Standard logic signals indicate the CR status information like filling, cooling, pocket status or start of a state machine in the FPGA of this module to generate action. Each action will force the system to write a slow control event into the output buffer to provide the corresponding status information in the data stream. Analog feed back from the pocket positioning system is fed into one of the FEBEX3B ADC channels and could be recorded in parallel. With this additional information even events during the insertion of the pocket can be analyzed to study extremely short-lived species. The major advantage of this concept is a completely independent run mode without time-consuming evaluation and combination of different data sources from data basis, external systems and the data acquisition itself.

Additional online monitoring will be performed by a WEB interface where the user can set and read slow control parameters. This WEB interface had been developed for the CsISiPHOS prototype and can be continued to be used in parallel.

5 Prototype experiment at the ESR

In a commissioning experiment the CsISiPHOS prototype was already tested in the ESR parasitic to an experiment to determine the half-life of hydrogen-like ^{142}Pm. The $^{142}Pm^{60+}$ ions were separated using the fragment separator (FRS), and then injected at an energy of 400 MeV/u into the ESR to be cooled and stored for decay measurements. An excellent resolution of $\Delta(\Delta E)/\Delta E = 0.9\%$ (FWHM) for the energy loss detectors and of $\Delta E/E = 0.5\%$ (FWHM) for the total energy measurement allowed for a clear separation of daughter nuclei $^{142}Nd^{59+}$, primary beam particles $^{142}Pm^{59+}$ which have picked up an additional electron, and a beam contamination of $^{138}Pr^{58+}$. In addition, the main components of different ion species had been well separated in the horizontal plane. This allowed for detailed comparison with ion optical calculations to verify the configuration of the ring. For the prototype the overall figures had been limited by the space limitation in the existing detector pocket which limited the number of silicon detectors and required the use of a 1 mm thick passive tantalum absorber in front of the CsI(Tl) crystal to stop the particles. The design of new detector pockets with a few millimeters more space for detectors in beam direction but also in vertical direction will definitely enhance the resolution and range of possibilities and are taken into account in the design of the future Collector Ring (CR) of FAIR.

The following sections give a short summary on the experimental details and the important results already published in [NDB+16].

5.1 Beam preparation and measurement cycles

A primary beam of ^{152}Sm was accelerated up to an energy of 550 MeV/u by the SchwerIonen Synchrotron (SIS18) at GSI Darmstadt, and impinged on a thick beryllium target at the entrance of the fragment separator (FRS) to produce secondary ions of interest. The H-like $^{142}Pm^{60+}$ ions were separated using the FRS [G+92], and then injected into the ESR to be cooled and stored for decay measurements. The primary physics goal of the experiment was the study of the recently-observed modulations in the electron-capture decay rate of H-like $^{142}Pm^{60+}$ and $^{140}Pr^{58+}$ [LBW+08]. A few hours of the beam time were assigned to the commissioning of CsISiPHOS by measurements of the β^+-decay of $^{142}Pm^{60+}$.

Neutral ^{142}Pm atoms ($Z = 61$) decay with a branching ratio of 96.4% to the ground state of the stable ^{142}Nd ($Z = 60$), while the remaining 3.6% of the decays end up in excited states [nnd]. CsISiPHOS was placed so that it only observes the β^+-decay products ($^{142}Nd^{59+}$) and the parent ions that pick up an electron in their atomic shells within the electron cooler ($^{142}Pm^{59+}$) (see figure 5.1). With the time-dependent rate of daughter ions we can determine the total decay constant of $^{142}Pm^{60+}$, since the decay rate is proportional to the total number of ions stored in the ring. But the decay rate observed by the detector is also influenced by the electron-capture rate to $^{142}Nd^{60+}$, because the decay rate is proportional

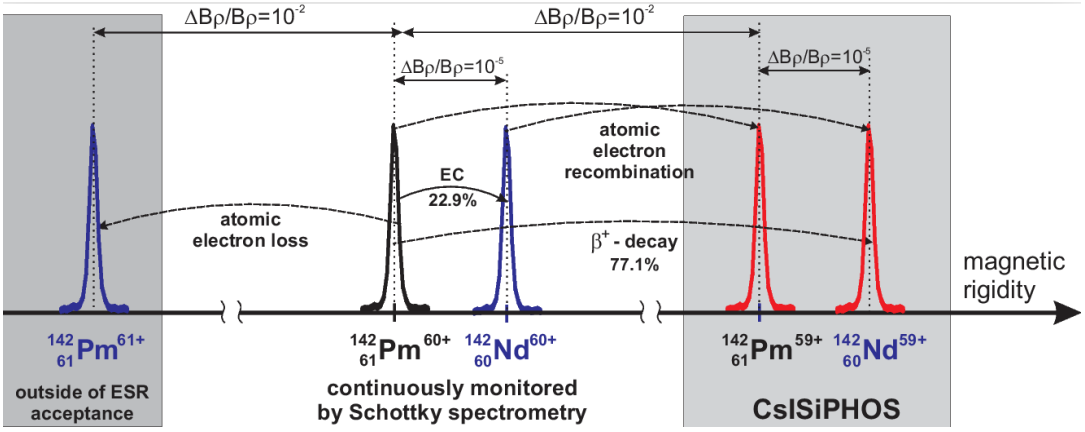

Figure 5.1: Possible decay channels in the experiment.

to the total number of ions stored in the ring. So the electron-capture rate has to be determined separately with the Schottky pickups.

During the commissioning of CsISiPHOS, a few tens of measurement cycles were performed. In each cycle, a few hundred $^{142}Pm^{60+}$ ions were injected into the ring, and after 3 s of stochastic cooling they were cooled further using the electron cooler. About 6 s after the injection, the detector pocket was moved towards the fully cooled beam until the front edge of the detector is 22 mm from the center of the beam pipe (this corresponds to a displacement of 89 mm in about 0.25 s). At this position, the shifted trajectories of the β^+-decay daughter ions, $^{142}Nd^{59+}$, hit the detector behind the vacuum window. A measurement period of 4 minutes was applied, during which most of the mother ions decay ($t_{1/2} = 39.2 \pm 0.7$ s [WGL+09]). At the end of each cycle (246 s after the injection) the ring was cleared of any remaining ions using a scraper, and prepared for the next cycle. A signal by any of the silicon pad sensors triggered the data acquisition system to record the event.

5.2 Detector configuration

The particle detectors in this experiment had to fit into the extremely tight pockets of the ESR, which are small rectangular stainless steel tubes with a cross section of 37×57 mm^2 (see Fig. 6.3). The vacuum of the ring is then separated from the air pressure inside the pocket by a window on the pocket that is usually made of a 25 μm stainless-steel foil. More information about the ESR detector pockets and their positions in the ring can be found in Reference [KK03].

For the most compact particle detector design, consecutive layers are mounted in alternating orientation. As additional advantages the sensor sides facing each other are supplied with similar electric potential and thus avoiding problems with leakage current or sparks in such a compact setup. Also a much more relaxed connector arrangement can be used with this solution. The passive degrader is a 1000 ± 8 μm thick slab of tantalum. All silicon sensors were vertically tilted by an angle of 3° with respect to the entrance window of the frame. This tilting reduces the influence of the silicon crystal orientation by the channeling effect [BBC+09]. Figure 5.2 shows the concept of this compact detector

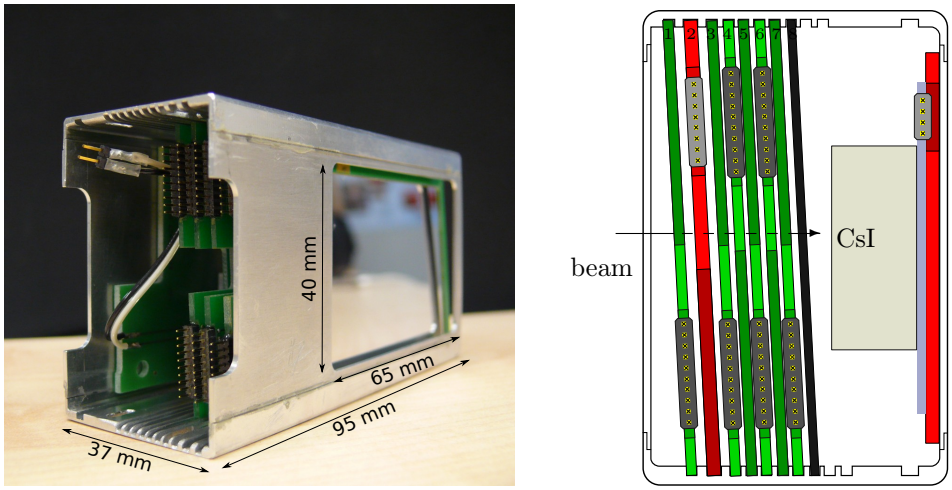

Figure 5.2: Left: Photo of the fully equipped detector. The entrance window has the dimensions 65×40 mm^2. Right: Schematic drawing of CsISiPHOS showing the arrangement of the sub-devices. The silicon sensors were tilted by 3° to reduce the channeling effect. The configuration of the sensors from left to right is given in the text.

design. The mechanical frame is machined from aluminum to guarantee a precise positioning of the elements in this drawer cabinet configuration. Bond wires sticking off the detector surface typically have a distance of 0.2 mm to their neighboring element in this configuration. The frame has 10 positions that can be filled with the individual sensor modules or passive degraders of suitable thickness. The configuration of the positions for the prototype experiment was as follows (the parenthesis indicates the silicon surface that faces the beam):

- Position 1: silicon pad sensor (n side) (see Section 3.1)
- Position 2: double-sided silicon strip detector, DSSD (p side) (see Section 3.2)
- Positions 3 – 7: silicon pad sensors (n/p/n/p/n sides, respectively)
- Position 8: passive degrader, tantalum (see Section 3.4)
- Positions 9 and 10: empty
- Positions 11: active stopper, CsI(Tl) crystal (see Section 3.3)

5.3 Energy resolution and particle identification

The calibration of the energy spectra is based on the calculation for the energy-loss of heavy ions using the ATIMA code [Wei]. Thanks to the use of the electron cooler in the ESR, the ion beams have a very low momentum spread $\Delta p/p$ and thus a well-defined kinetic energy, in our case 400 MeV/u. Using this value, the calculated energy-loss values were compared to the ADC values read out from the detector channels. The ADC offsets were derived from an electronics calibration using a pulse generator connected to each detector channel.

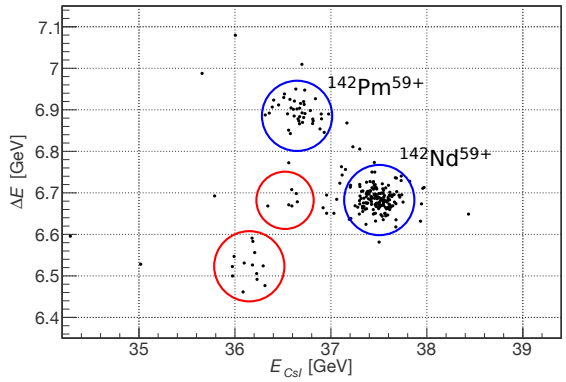

Figure 5.3: Energy loss in silicon pad sensors, ΔE, versus CsI(Tl) energy, E_{CsI}. For explanation, see text.

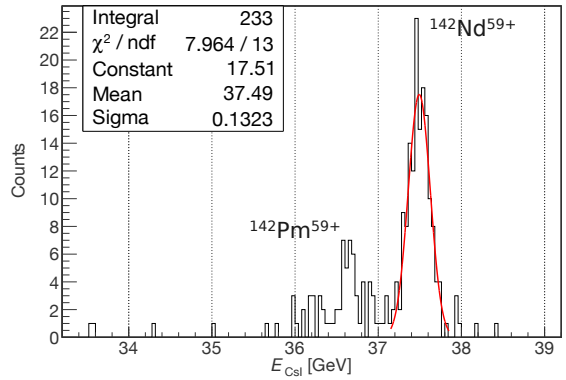

Figure 5.4: Energy spectrum of the CsI(Tl) scintillator. The red curve is a Gaussian function fitted to the histogram.

After calibration, the energy signals of the silicon pad sensors (E_i) were summed event-by-event to obtain $\Delta E = \sum_i E_i$. Due to the position dependent resistor chains for the readout of the DSSD this sensor was excluded from the sum to improve the ΔE resolution.

The measured energies in the active stopper (the CsI(Tl) scintillator) are also used for particle identification after using the same calibration procedure. The histogram of the energy loss in the silicon pad sensors, ΔE, versus the energy of CsI(Tl), E_{CsI}, is shown in Fig. 5.3, in which these two groups of events ($^{142}Nd^{59+}$ from β^+-decay and $^{142}Pm^{59+}$ from electron-pickup) are indicated by blue circles and can be clearly distinguished. The red circles in Fig. 5.3 show a few unexpected events whose origin are still unknown.

In addition, there are two groups of events shown with red circles. These events might have been produced via the stochastic cooling, which has a limited acceptance for the revolution frequencies. If the revolution frequency is outside the acceptance, the stochastic cooling causes the ions to heat up. The heated ions can be stored in the ring for a short time, and eventually recombine with electrons through collisions with the rest gas or in the electron cooler and thus hit the detector.

Figure 5.4 shows the energy spectrum of the CsI(Tl) scintillator, with a main peak at 37.5 GeV which is from $^{142}Nd^{59+}$ ions, and a smaller peak at lower energies of 36.6 GeV,

Table 5.1: The measured and calculated energy losses in the sensors for $^{142}Pm^{59+}$.

Sensors	$E_i^{experiment}$ [GeV]	FWHM [GeV]	FWHM^{ATIMA} [GeV]	E_i^{ATIMA} [GeV]
Pad sensor 1	1.12	0.02	0.022	1.12
DSSD	0.68	0.02	0.013	0.68
Pad sensor 2	1.14	0.03	0.022	1.14
Pad sensor 3	1.15	0.03	0.022	1.15
Pad sensor 4	1.16	0.03	0.022	1.16
Pad sensor 5	1.17	0.03	0.022	1.17
Pad sensor 6	1.18	0.02	0.021	1.18
CsI(Tl)	37.5	0.30	0.090	37.5

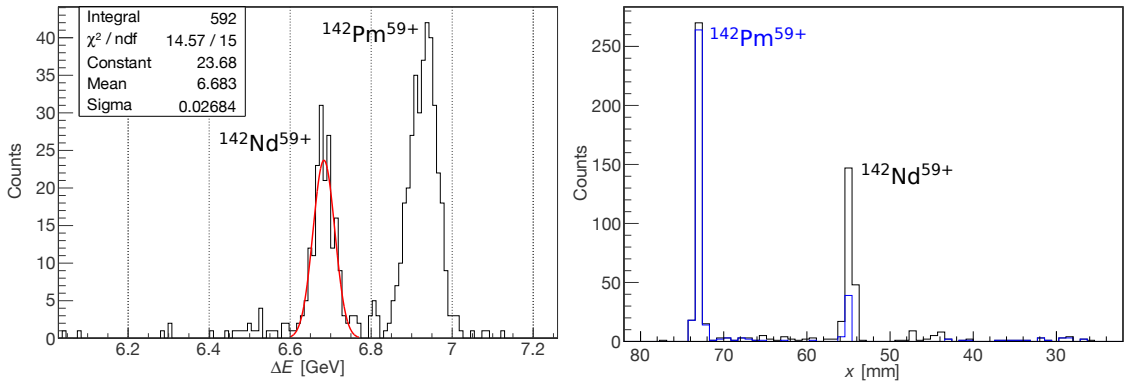

Figure 5.5: Left: Energy loss spectrum of the silicon pad sensors, $\Delta E = \sum_i E_i$. The red curve is a Gaussian function fitted to the histogram. Right: Position histogram of the ions on the DSSD in the ESR coordinate system. The blue histogram represents the events with a condition on the energy loss, namely $\Delta E > 6.8$ MeV.

which is from the recombined parent ions, $^{142}Pm^{59+}$. Although Fig. 5.5 indicates that the $^{142}Pm^{59+}$ ions do not normally hit the CsI(Tl) scintillator, which covers the x-range from about 52 to 76 mm, their trajectory is close to it, and it is possible that some ions are scattered and then hit the CsI(Tl) crystal.

The energy loss histogram, shown in the left panel of Fig. 5.5 in black, has two peaks which are created by the β^+-decay products ($^{142}Nd^{59+}$) and by the $^{142}Pm^{60+}$ ions that recombine with an electron in the electron cooler ($^{142}Pm^{59+}$). Since the energy loss of ions at this velocities scales approximately with the square of their atomic number, Z^2, the peak at higher energies can only be from the recombined parent ions, $^{142}Pm^{59+}$. The blue histogram in the right panel of Fig. 5.5 shows the events with a condition on the energy loss, namely $\Delta E > 6.8$ MeV. It appears that the $^{142}Pm^{59+}$ ions hit two different positions on the DSSD, depending on the position of electron recombination.

The position of the pocket was adjusted so that the β^+-decay daughter ions, $^{142}Nd^{59+}$, hit CsISiPHOS roughly at the centre of the sensitive area. Looking in the direction of the beam momentum, this adjustment puts the centre of the DSSD at $x = 52$ mm in the ESR frame, which is a right-handed Cartesian coordinate system with z axis in the

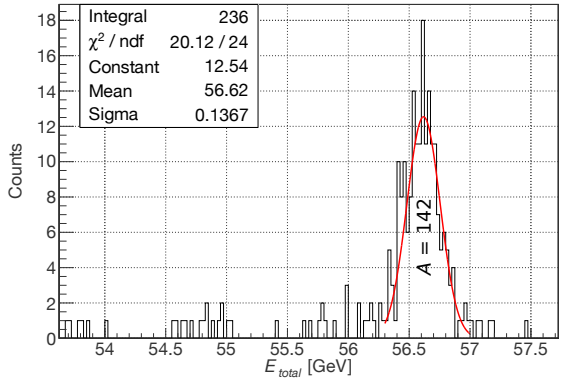

Figure 5.6: Total energy reconstruction, $E_{total} = \Delta E + E_{DSSD} + E_{Ta} + E_{CsI}$. The energy loss in the entrance foil of the pocket is around 160 MeV, which is not added to this sum.

beam direction and origin on the central axis of the ESR beam pipe. CsISiPHOS detects $^{142}Nd^{59+}$ and $^{142}Pm^{59+}$ ions at distances of approximately 54 mm and 73 mm from the centre of the beam pipe, respectively.

Fig. 5.6 shows the total energy spectrum, obtained by summing the energy loss of the beam in all components of CsISiPHOS, event by event: $E_{total} = \Delta E + E_{DSSD} + E_{Ta} + E_{CsI}$. To avoid systematic uncertainties the energy loss of the particles in the tantalum degrader, E_{Ta}, was extrapolated from the measured energy loss in the silicon pad detectors, ΔE, by a constant scaling factor R, for each element. From a detailed ATIMA calculation, the average energy loss of $^{142}Nd^{59+}$ in six layers of silicon pad detectors was determined to derive R as the ratio of the energy loss in Ta from ATIMA (E_{Ta}^{ATIMA}) and the sum of energy losses in the silicon pad detectors from ATIMA (ΔE^{ATIMA}),

$$R = \frac{E_{Ta}^{ATIMA}}{\Delta E^{ATIMA}}.$$

Then we calculate $E_{Ta} = R \cdot \Delta E$ per event.

The energy resolution values for CsISiPHOS have been determined by fitting Gaussian distributions to the spectra, giving:

$$\begin{aligned} \text{FWHM}(\Delta E): &\quad 60 \text{ MeV at 6.7 GeV} \\ \text{FWHM}(E_{CsI}): &\quad 0.3 \text{ GeV at 37.5 GeV} \\ \text{FWHM}(E_{total}): &\quad 0.3 \text{ GeV at 57.0 GeV} \end{aligned}$$

With this resolution the neighboring ions in the range of interest are well distinguished. The electronic noise of each silicon pad detector is around 3 MeV FWHM, and the combination of the CsI(Tl) and the silicon photo-diode has an electronic noise of around 30 MeV FWHM. The energy loss variations due to the distribution of incidence angles are negligible, because the incidence angle of the decay ions is smaller than 0.17° (see Fig. 5.7).

The ATIMA calculations give an energy straggling of around 33 MeV in the Ta absorber, and since E_{Ta} was determined by scaling ΔE, the uncertainties from ΔE are multiplied by a factor of 1.8. Nevertheless, the straggling in the Ta absorber remains a small contribution to the total energy resolution of 300 MeV FWHM. This indicates that probably the energy

resolution in the CsI(Tl) detector is the limiting factor. Due to the compact geometry and the difficult wrapping of a rectangular scintillator on a round shaped silicon photo-diode, it is likely that the light collection was not homogeneous. Also the strong nonlinearity of the energy loss, the quenching factor for heavy ions in CsI(Tl), and the stopping close to the surface of the photo-sensor may have limited the absolute resolution achieved. Especially the latter one should be relaxed in future experiments by using a wider pocket that also allows for using a much thicker layer of scintillator material.

The observed ΔE resolution $d(\Delta E)/\Delta E = 0.9\%$ corresponds to a Z resolution of $dZ/Z = 0.45\%$ or $dZ = 0.27$ (FWHM) for separation of elements around $Z = 61$. As a constant resolution for separation of elements up to $Z = 81$ is expected this is about a factor of two better than the results obtained in the work of L. Maier, $dZ = 0.55$ (FWHM) [Mai07].

CsISiPHOS can stop ion of Tl and heavier at 400 MeV/u without a passive absorber, and the Ta absorber can be replaced by a silicon pad detector in such experiments. Therefore, for the future measurement of the bound-state β-decay rate of ^{205}Tl a better performance is expected.

5.3.1 Beam Simulations

Currently there is no high resolution monitor for the beam profile installed close to the measurement position of the CsISiPHOS detector. Therefore the parent beam trajectory cannot be determined accurately from the ESR configurations. However, ion-optical calculations can be used to calculate the trajectory of the parent ion beam as well as the trajectories of the decay products. These calculations can then be compared to the measurements of CsISiPHOS to improve our understanding of the optical models of the ESR and later also for the CR.

The ion-optical calculations of the ESR for this experiment are shown in Fig. 5.7. The horizontal axis shows the path length of the ion beam for one orbit (the ESR circumference is 108.36 m). Light and dark grey bars indicate dipole magnets and the electron cooler, respectively, and the small yellow rectangle at about 80 m shows the CsISiPHOS position. The trajectory of the parent ions is indicated with a dashed black line. The coloured bands illustrate the beam trajectories when a β^+ decay to ^{142}Nd^{59+} or a recombination to ^{142}Pm^{59+} occurs. The width of the bands reflects the uncertainties of the trajectories caused by a combination of two effects, the uncertainties in the magnetic fields and different locations of the decay or recombination along the beam axis. The measured trajectory is expected to be within the width of the band which is not related to the width of the measured position spectrum.

Four different cases have been calculated:

- ① if the parent ion recombines with an electron in the electron cooler, the trajectory of the ^{142}Pm^{59+} ion will be as shown with the green band.
- ② if β^+-decay occurs in the straight section of the electron cooler, the trajectory of the daughter ions, ^{142}Nd^{59+}, is the same as case ①, shown with the magenta band.
- ③ if the β^+-decay occurs in the straight section between ∼52 and 70 m, the daughter ions travel along the red band.

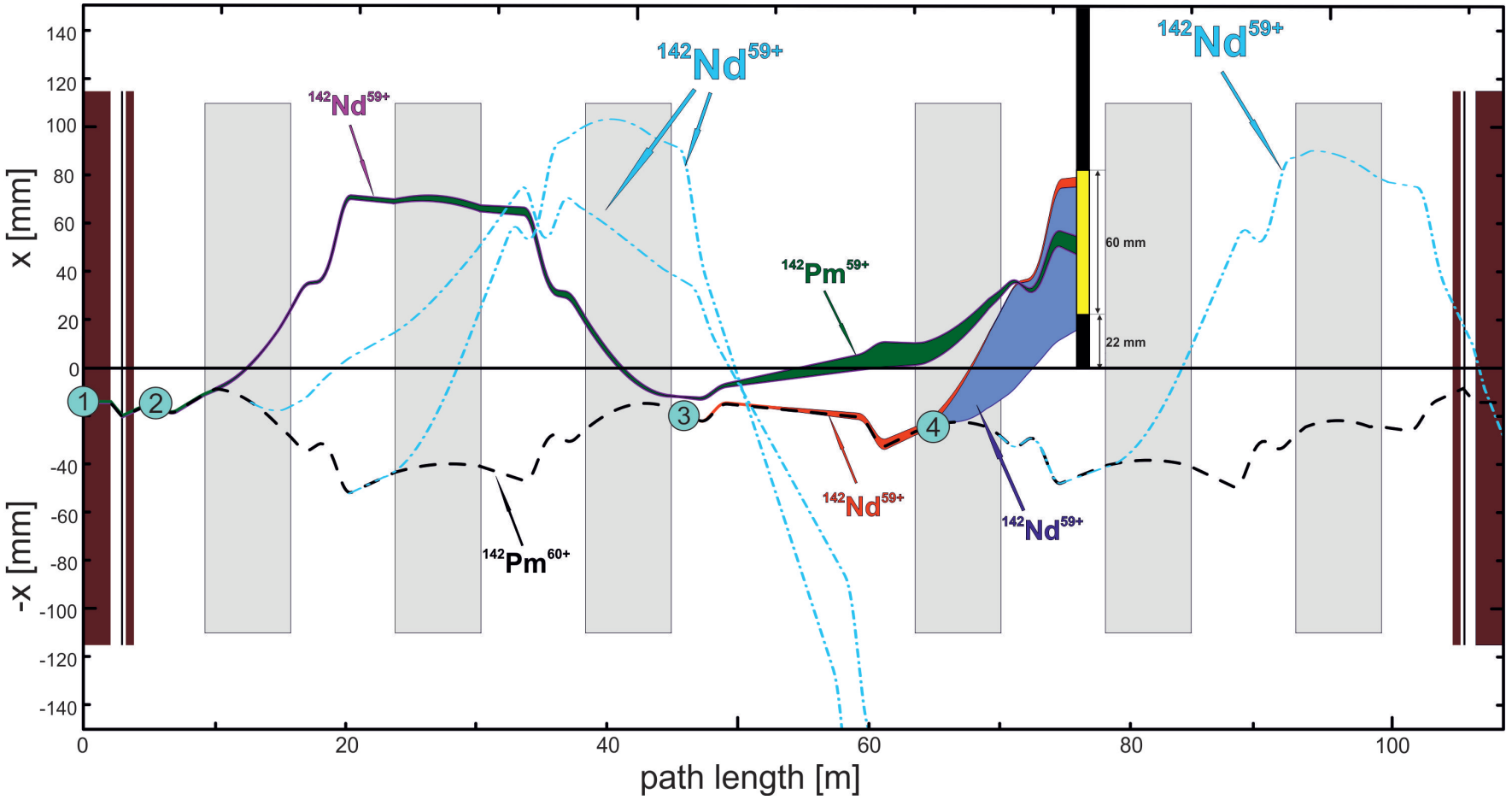

Figure 5.7: Ion-optical calculation of the beam trajectories. Light grey bars indicate dipole magnets, the dark grey ones show the electron cooler area, and the yellow bar at about 80 m shows the position of CsISiPHOS. Not shown are the quadrupoles and higher-order correction magnets. The explanation of different decay cases numbered from 1 to 4 is given in the text.

- ④ if the β^+-decay occurs in the first half of the dipole just before the detector, the trajectory of the daughter ions is within the blue band. The cyan dashed lines show a few examples of the daughter ion trajectories when the decay occurs in places other than the above four cases. Those events are not detected and are lost.

These four cases cover all relevant cases for this experiment. If the parent ions decay in a position other than the above cases, the decay products will go out of the acceptance of the ring without an interaction with the detector (see cyan dashed lines).

The ion-optical calculations verify that the parent ions recombined with an electron in the cooler region hit the detector (green band). In addition, the decay products, $^{142}Nd^{59+}$, generated in any of the straight sections of the ring (positions ② and ③ in figure: 5.7) have a chance to be detected.

Although the calculations nicely reproduce to the measured positions, there is room for improvement, especially for the relative distance of the trajectories at the position of the detector. The green and red trajectories in Fig. 5.7 have a relative distance of nearly 2.6 cm on the detector, while the measured value is 1.9 cm (right panel, Fig. 5.5). Adjusting the beam optics models could improve the calculations to agree with the measured positions. Further developments of the calculations for the ESR are beyond the scope of this TDR, and will not be discussed here. But it is clear that this kind of direct comparison allows for a precise understanding of the magnetic lattice which will be of utmost importance when commissioning the CR.

6 Mechanical Structure and detector position in the CR

It is important that the detectors are placed at positions with enough dispersion to separate the circulating beam and ions which changed their charge after β decay. But on the way to the detector the dispersion must also not be larger, otherwise only poor transmission to the detector can be reached.

As discussed in chapter 1 a position in the CR behind two dipoles is well suited for detection of charge change in the region around Z=50, and after four dipoles for Z around 82. Therefore, the vacuum tubes at these positions will not be simple tubes but crosses, as shown in Fig. 6.2. The detector pockets will then be mounted on CF150 flanges left or right to the beam. When not in use the CF150 ports are closed by a simple blind flange. The names of the exact locations in the CR are: CR01EX3SZ, CR01EX4SZ, CR03EX3SZ, and CR03EX4SZ. In some places the detector positions are the same as foreseen for Schottky pickups which are also from the ILIMA collaboration. In this case the cross has to be exchanged with a Schottky pickup later. It is not planned to use both detectors at the same cross at the same time.

In the following sections the pockets along with drives and a support will be discussed in detail. Especially the UHV mechanics and the control units according to FAIR standards contribute the major part to the overall costs of the project (with PSP 1.2.6.5.).

6.1 Mechanical Concept

The basic requirements for the mechanical layout of the detector setup discussed in Chapter 2 are summarized here.

- The detector has to be inserted from its parking position to the measurement position within a single second.
- The absolute precision of the detector position has to be better than 1 mm in both directions perpendicular to the beam line.
- For the extraction of the detector from the measurement position to its parking position a flexible time window of up to 5 seconds is reasonable.
- The pocket window has to be protected from any mechanical stress.
- There should be no extra forces on the beamline during the detector operation.

To fulfill all these requirements a rather massive mechanical frame as shown in Fig. 6.2 will be installed. This guarantees a minimum of deformation while not transmitting any additional force to the vacuum system of the beamline. The high speed requirements for the injection into the beamline, the large diameter of the vacuum bellow and thus the

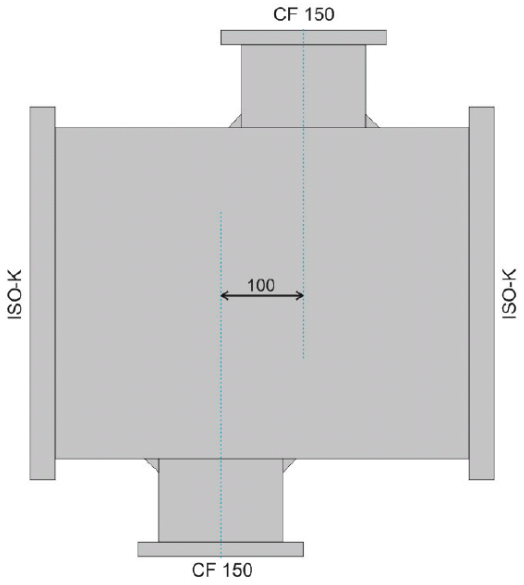

Figure 6.1: Scheme of the vacuum cross, with CF150 ports to the sides and ISO-K flanges with an open diameter of 400 mm along the ring. The two side ports are shifted by 100 mm.

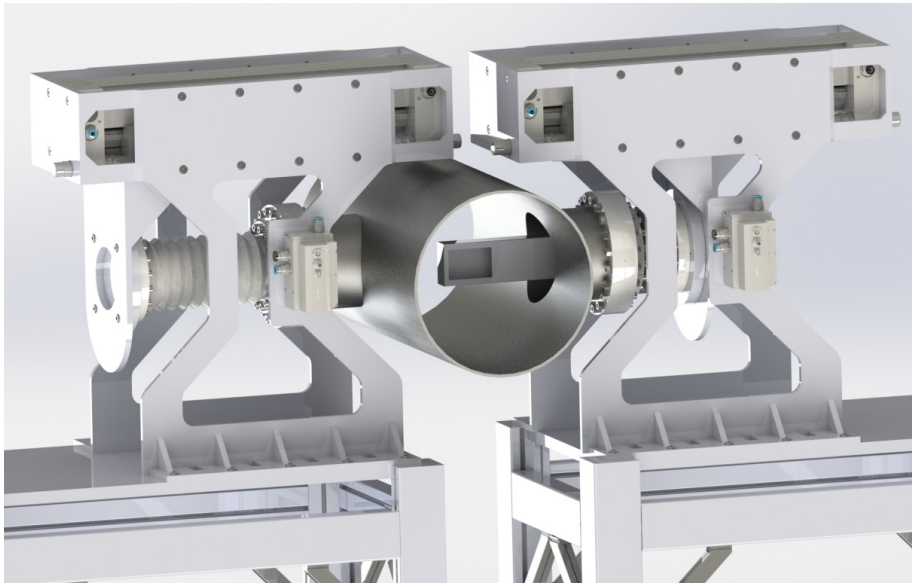

Figure 6.2: Model (Solid Works^{TM}) of the full detector mechanics. The massive mechanical support allows for a fast and precise injection of the detector pockets to their measurement positions.

resulting forces, and the limits for vibrations and acceleration for the fragile detectors strongly constrain the choice of the drives to be eligible.

Standard FAIR step-motor drives using "Oriental Motor NanoStep RFK-Series" and control units from Cosylab were excluded due to their limit in the product of torque and rotation frequency. Also other step-motors from different companies were investigated but

limit the total injection time to less then 3 seconds. Pneumatic drives like currently used at the ESR would be an optional solution. In combination with an additional low step-motor drive for the offset adjustment this provides sufficient flexibility for the standard operation. Major disadvantages of such a solution is the more complicated interfacing of two systems, and a time consuming calibration procedure each time the total path length or the driving speed is changed.

For the most flexible, safe, and cost effective operation we have chosen an electro-mechanical solution based on a servomotor drive from FESTO. This system can be operated up to a speed of 2 m/s with a maximum torque of 680 Nm on the carriage and an accelerating force of 1300 N with a repeat accuracy of 20 μm. A powerful motor with 1.05 kW power offers a minimum of injection time of half a second. Digitally adjusted ramping provides continuous acceleration and deceleration for each cycle to protect even fragile detectors mounted. Built-in motor breaks guarantee a stable position in case of any power failure. An additional encoder built into the drive provides a position feedback with 10 μm precision also used for a hardware interlock. In addition two gas cylinders for massive damping will be mounted on both ends of the drive to avoid damage in case of user-induced operating error.

In addition to the hardware interlock systems the motor control provides a continuous power monitoring. If the motor current exceeds a programmable limit an automatic shut-down procedure is initiated.

The vacuum part of the mechanics is provided by MetalFlex. A 450 mm long bellow with an opening diameter 100 mm can be compressed to its minimum length of 150 mm within 0.2 seconds. The hardware limiters of the drive make sure that these limits warranted can never be exceeded. This device is welded to standard CF100 UHV flanges on both sides. Using copper sealing they are specified to permanent baking temperatures of 230 °C. During the baking procedure the detector will be dismounted and the mechanical parts of the drive will be shielded by an optical reflector and a copper heat spread mounted between the vacuum bellow and the rail system of the drive. For this operation the drive has to be moved to the most backward position. The top plate of the drive housing will temporarily get a water cooled jacket fixed from the top with a conductive rubber heat transmitter in between. Calculations for the heat transport have shown that under these conditions using cooling water of 20 °C the drive will not exceed a temperature of 100 °C.

6.2 Detector pocket for the CR

The design of the heavy ion detector for the CR is based on the CsISiPHOS design discussed in chapters 3 and 5. Major difference here will be a change of the depth of the vacuum pocket in beam direction to avoid the use of passive degraders in most experiments. Here the opening length in beam direction has to be extended from 37 mm to 58 mm to allow for the use of a thicker active stopper for the ions. Also the opening diameter in vertical direction should be slightly modified from 56 mm to 58 mm to allow for a more robust detector main frame, which would simplify the detector mounting and the precision of the detector positioning. Both changes do not introduce a change in the opening diameter of the vacuum bellow which would increase the mechanical forces and therefore also the complexity of the drive. Neither the size of the vacuum window nor the window thickness itself has to be changed. The new pockets are expected to have the same excellent performance

as the existing one, being in operation for nearly a decade now in the ESR (see Fig. 6.3). With this strategy major additional development costs can be avoided.

Mounting and dismounting of individual pockets will be a major effort. A full section of the ring has to be flushed, parts have to be mounted, checked for leakage rates, and then the whole section has to be baked to reach the UHV conditions again. Such operations will not be possible on a regular basis and should be avoided to a large extent. Therefore the ILIMA collaboration plans to have four complete mechanical stations with pockets and the hardware parts of the drives to get a full arc of the CR equipped for the different experimental options. The detector itself will be easy to change from one pocket to another as the inside of the pocket will be at air pressure just flushed with dry nitrogen to avoid any detector aging. The same holds true for the drive control and the data acquisition system which will be mounted in a mobile rack system. This concept slightly increases the investment of the mechanics but will allow for a continuous operation of the device without influencing the scheduling process for experiments.

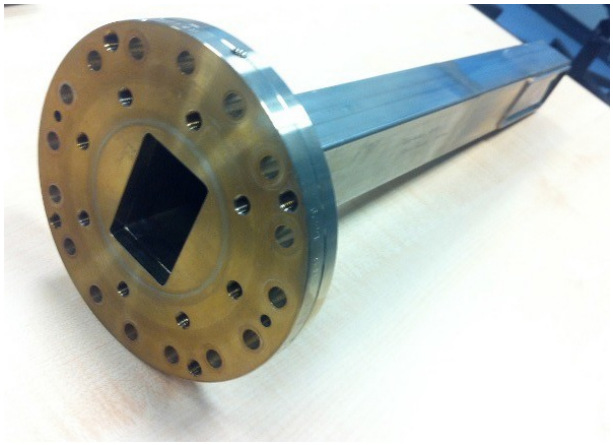

Figure 6.3: The existing detector pockets at the ESR have proven highest reliability and will be just slightly modified to fit the requirements of the CR.

6.3 A compact detector module

The CsISiPHOS detector concept (see chapter 5) has proven an excellent performance, an easy and reliable handling and sufficient flexibility to be applied to all experiments currently foreseen in the ILIMA program. Especially the rail concept to insert the different detector units in a drawer-like structure has proven a precise positioning of any random detector configuration. The minor changes in the pocket design as discussed in Section 6.2 will first of all increase the active detector length but also relax the tight constraints for the detector mounting and especially the window protection. All other parts will be produced according to the design of CsISiPHOS shown in Section 5.2.

7 Radiation Environment and Safety Issues

The radiation dose that the heavy ion detector is exposed to is limited by the number of particles stored in the ring and their half life. Upper limits are given by the expected 10^6 particles stored and a half life similar to a filling and measurement cycle of 10 seconds. With a geometrical acceptance of about 20% of the total ring circumference it can thus be estimated that the heavy ion detector will suffer a maximum rate of 2×10^4 particles/s projectile-like reaction products. Please note, that many of the experiments will focus on very rare ions (down to 10 particles) in the ring. Therefore a mean value of 10^3 beam ions and equivalent 2×10^1 particles/s are taken into account for the estimation of the overall dose on the telescope. With an operation time of 2 months per year, 5×10^6 particles/cm^2 per year are estimated to pass the active volume, neglecting duty cycle. Occasionally emitted neutrons will not be thermal and thus pass through the detector with low probability of activating the material. More abundant radiation such as X-rays and delta electrons have even less impact on the material used. In case of unforeseen operation modes of the ring or pockets being injected into the beam line during the filling, the geometrical coverage of the pocket prevents non-reacted beam particles from hitting the detectors. Even an unexpected change of the magnet setting will not influence the detector as the particles will be scraped off by the massive edge of the pocket. Beam monitoring in the ring will automatically indicate such massive losses and stop the operation in such unexpected states to avoid activation of the pocket. Radiation damages as well as aging for the silicon detectors as well as for the electronics close by therefore can be excluded. During operation the activation will be continuously monitored by the detector itself. After use the detector will be extracted off the pocket and stored outside the radiation area. The silicon used for in the heavy ion detector requires a high-voltage supply, up to 500 V. Each channel is individually protected with a current limit of 20 μA. Standard operation procedures according to VDE[1] will be followed to guarantee the safe operation of the entire electric installation.

The detector operation requires the use of dry nitrogen at a maximum rate of 100 l/h as a flushing gas to protect the detector against humidity. This will not significantly affect the oxygen concentrations in both the large volume and the non hermetically closed experimental hall. Therefore, connection to a special exhaust system are not required.

The detector mechanics is basically split into two independent (left and right) parts which can be moved in the experimental area using standard wheels temporarily mounted to the base frame. For transport and storage, additional bars are required to be mounted on the floor level; expanding the base area to 1 x 1 m^2 to avoid any tilting of the rather high frame structure.

[1] VDE, the Association for Electrical, Electronic & Information Technologies, German: Verband der Elektrotechnik Elektronik Informationstechnik e.V.

8 Infrastructure

The heavy ion detector for ILIMA basically is the combination of two important components. The sensor device with its readout electronics and the vacuum system with the UHV pocket and its mechanical installation.

The sensor device is mobile and will be moved between the pockets. This is a fast operation performed within one day. Also the corresponding electronics rack will be mobile. As discussed in chapter 4 only standard connections are needed. Total power consumption will not exceed a limit of 3 kW which allows for air cooling inside the experimental hall. Power will be drawn through 4 standard power plugs from the measurement grid. In addition the rack will need two gigabit network connections, a glass fiber access for the White Rabbit time stamping switch and connetion to the accelerator control unit which provides digital signals for the beam injection and cooling cycles. This infrastructure has to be provided at all four optional measurement positions CR01EX3SZ, CR01EX4SZ, CR03EX3SZ, and CR03EX4SZ along the ring.

The pocket drives mounted at this positions are controlled by an industrial PC also mounted in the electronics rack. If not in use or disconnected the drives are blocked automatically and stay at their latest position. The motors are driven by a local power units which need an additional power connection to the grid. In addition each detector position along the ring has to be equipped with a connection to the dry nitrogen supply (0.3 bar $<$ p $<$ 6 bar) to flush the detector pockets. A standard connection to the pressured air (3 bar $<$ p $<$ 10 bar) should be available to supply an optional damping systems for future upgrades which may allow for even faster insertion of the pockets.

For the baking procedure during the initializing of the CR a connection to the cooling water (temperature T $>$ 15°C) will be used. The typical water througput according to the heat load of 1 kW will be 100ml/s. This will be used in short periodes of a few days per year only. The total weight of the each pocket drive system will not exceed a limit of 100 kg. Even not required for safety reasons a crane access is recommended for the mounting procedure.

9 Installation Procedure

The installation of the pocket systems is an intervention into the UHV system and has to be performed in close collaboration with the CR team. Breaking the ring vacuum is a time and manpower consuming procedure which can only happen few times. During the setup of the CR the interface elements (see chapter 6) will be already installed but covered with blind flanges. After the first successfull vacuum test of the CR when the first active elements will be installed, four of the pocket systems have to be installed in one of the arcs of the CR, while the other four interface elements stay closed, or will be used by the Shottky sensor units.

In a first step the four support tables made from light weight ITEM aluminum profiles will be mounted, aligned and fixed to the floor.

Extensively tested UHV units of pocket and bellow will be mounted by the CR vacuum team supported by experts from the ILIMA collaboration. The flanges of the stainless steel bellows containg the pockets will be connected to the drive system on both sides to avoid any forces to be transmitted to the ring vacuum system during operation. During the first baking procedure all units will be monitored to avoid any overtemperature related to the heat jackets. For safety reasons the pockts will be flushed with dry nitrogen during the baking procedure. After dismounting the heat jackets the pocket system is operational. In first tests the empty pockets will be moved in and out to make sure that the heating did not affect any of the elements. If this operation is confirmed, the drive system has to be tuned to the different insertion speeds and the absolute lateral positions will be calibrated. Calibrated motor parameters will be stored in the drives and for backup also at the FAIR control data base. In a next step a dummy detector system will be inserted to each pocket to measure the local acceleration at the detector positions. For the insertion of any system into the pocket a rail system inside guaratees that no element inserted can touch the fragile vacuum window under stress. This rails also allow for a precise positioning of the detector units. The precise position of the detector within the pocket and relative to the beam line is checked using fixed points on the mounting structure (see section 6). The mounting procedure will be finished after all the pocket units have been tested, calibrated and seald with protection flanges.

10 Time Schedule and Organisation

We summarise in this chapter the organisation of the heavy ion detector Working Group and the time schedule for the project. For simplicity, we show here only names of participant institutes with the coordinates of a contact person.

10.1 Time schedule and Milestones

The construction of the prototype detector has been finished and the results of the first experiment with this device are shown in chapter 5. This detector will be extended for the FAIR Phase-0 experiments planned for the years 2018/19 to cover the full active area with a larger active stopper based on CsI(Tl).

For the implementation of the full size detector array in the CR three workpackages have been defined.

- Design of the extended detector version, implementation and test of further sensors.
- Implementation of high density BGO, GGAG, GYGAG (or other) new scintillator materials with a higher density and similar light output.
- Construction and assembly of the pocket stations including the motor drives, control and interface.
- Construction and testing of the enlarged pocket units based on the established foil soldering/welding technique.

The overall time plan for this work packages is dictated by the CR installation plan with a start of comissioning of the vacuum system in Q3 2022. Here work packages 3 and 4 have to be finished and all four pocket stations have to be inserted to the CR after a first successful rough vacuum test of the giant UHV tube system at ring being installed. All mechanical tests have to be performed during that period to allow full operation of the CR.

With stable beams in the CR already beginning of 2023 the heavy ion detectors could be commissioned with any stable beam in the ring. Electron pickup from the residual gas will produce sharp peaks of ion impacts on the detectors when changing their A/Q on the straight sections of the storage ring.

As all the workpackage items are based on developments which had been sucessfully completed as a prerequisit for this TDR, a periode of 3 years is foreseen for completing all work-packages. According to this dead-lines all partners of the working group have enough time to collect the corresponding funds listed in chapter 11.

Figure 10.1 summarizes the time schedule for this enterprise including the most important milestones.

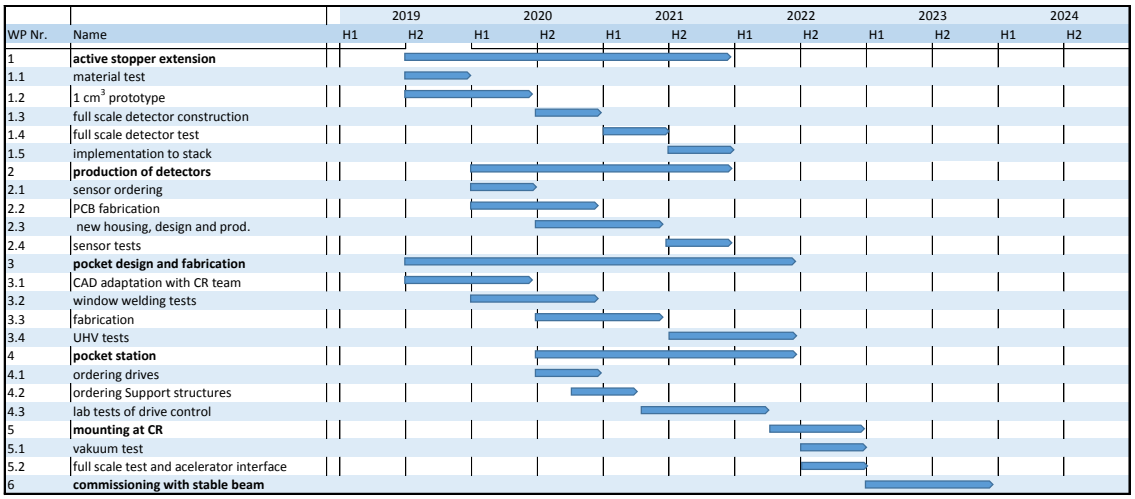

Figure 10.1: Time schedule of the production and installation of the heavy ion detector units

10.2 Organisation and responsibilities

The R&D work summarised in this document has been shared between four institutions over a period of 5 years. The participants in this working group are:

GSI Helmholtzzentrum für Schwerionenforschung, Darmstadt
N. Kurz, S. A. Litvinov, Y. A. Litvinov, A. M. Najafi, S. Sanjari, H. Weick,

JLU Justus-Liebig-Universität Gießen
A. M. Najafi, I. Dillmann (-2013)

TRIUMF Canada's national laboratory for particle and nuclear physics and accelerator-based science
I. Dillmann

TUM Technische Universität München
M. Böhmer, T. Faestermann, R. Gernhäuser, L. Maier, S.Winkler

For the future the Saitama University group around Takayuki Yamaguchi pointed out a strong interest to join the working group for the development and implementation of the scintillation detectors.

11 Costs and Fundings

In order to prepare the realization of the detectors including the infrastructure, the different costs have been calculated and the expected funding amounts and sources are summarized in this chapter.

11.1 Summary of the expected Costs

The following tables summarizes the estimated cost of the ILIMA heavy ion detector (FAIR PSP code 1.2.6.5). We start by presenting in table 11.1 an overview that includes all the costs associated to this device, mentioning only general items.

The costs for the prototype CsiSiPHOS amounted to about 100 k€ and are basis of the cost estimates shown here. In the following tables the additional costs for the CR implementation are listed. For the full operation two detector units are needed to cover either of the two bins in magnetic rigidity on one side of the ring or the two sides of one plane along the ring reserved in each of the interface flanges. The device will consist of two major components: two detector stacks with their corresponding readout electronics and four drive systems with the pockets injected into the ring. All costs are given in 2017 equivalent including VAT.

Vacuum drives and frame mechanics	45 k€
Data acquisition and slow control	47 k€
Detector pockets and UHV bellows	44 k€
Detector stack with interface	65 k€
TOTAL	**201 k€**

Table 11.1: Summary of the expected costs for the heavy ion detectors Detector

11.2 Funding scheme

The ILIMA heavy ion detector will be funded within the ILIMA collaboration according to the ILIMA money matrix. This matrix summarizes the intention to raise funds in order to finance the detection system. Table 11.6 summarizes the values corresponding to September 2017. In addition values corresponding to the year 2005 are given in which the technical proposal was approved by the CORE committee. For the adaptation an escallation factor of 1.4 has been applied.

Item	Nr. of units	Cost per unit	Total
FESTO drive unit 120	4	3.2 k€	12.8 k€
Motor unit	4	1.4 k€	5.6 k€
Base frame ITEM	4	2.4 k€	9.6 k€
Drive frame	4	3.0 k€	12 k€
Controler unit FESTO	2	1.5 k€	3 k€
Cableing	4	0.5 k€	2 k€
TOTAL			**45 k€**

Table 11.2: Details of the expected costs associated with the motor drives and the mechanics

Item	Nr. of units	Cost per unit	Total
Preamplifier MPR16	2	2.8 k€	5.6 k€
Amplifier MSI8	2	3.6 k€	7.2 k€
HV Module MHV4	3	4.1 k€	12.3 k€
FEBEX DAQ system	2	9.5 k€	19.0 k€
Industry PC	1	2.5 k€	2.5 k€
Cableing	1	0.4 k€	0.4 k€
TOTAL			**47 k€**

Table 11.3: Details of the expected costs associated with the data acquisition and slow control

Item	Nr. of units	Cost per unit	Total
Detector Pocket CF100	4	2.8 k€	11.2 k€
Foil welding incl. tests	4	3.0 k€	12.0 k€
Welded bellows CF100	4	3.6 k€	14.4 k€
Sealing and mounting	4	0.4 k€	1.6 k€
Flanges and gas connections	16	0.3 k€	4.8 k€
TOTAL			**44 k€**

Table 11.4: Details of the expected costs associated with the detector pockets and UHV bellows

Item	Nr. of units	Cost per unit	Total
Pad detectors	10	4 k€	40 k€
DSSDs	2	4.8 k€	9.6 k€
Active stopper BGO	2	1.9 k€	3.8 k€
Active stopper PD	4	2.4 k€	9.6 k€
Detector mechanics	1	2.0 k€	2.0 k€
TOTAL			**65 k€**

Table 11.5: Details of the expected costs associated with the detector unit

Item Partner	costs (2017)	cost (2005)
Detector pockets and UHV bellows TRIUMF	44 k€	31.4 k€
Vacuum drives and frame mechanics Data acquisition and slow control GSI Helmholtzzentrum für Schwerionenforschung	92 k€	65.7 k€
Detector stack with interface Technische Universität München	65 k€	46.4 k€
TOTAL	201 k€	**143.5 k€**

Table 11.6: Summary of the funding matrix for the heavy ion detector

References

[BBC+09] L. Bardelli, M. Bini, G. Casini, G. Pasquali, G. Poggi, S. Barlini, A. Becla, R. Berjillos, B. Borderie, R. Bougault, M. Bruno, M. Cinausero, M. D'Agostino, J. D. Sanctis, J. Dueñas, P. Edelbruck, E. Geraci, F. Gramegna, A. Kordyasz, T. Kozik, V. Kravchuk, L. Lavergne, P. Marini, A. Nannini, F. Negoita, A. Olmi, A. Ordine, S. Piantelli, E. Rauly, M. Rivet, E. Rosato, C. Scian, A. Stefanini, G. Vannini, S. Velica, and M. Vigilante. Influence of crystal-orientation effects on pulse-shape-based identification of heavy-ions stopped in silicon detectors. *Nucl. Instrum. Meth. A*, 605(3):353 – 358, 2009.

[BFF+96] F. Bosch, T. Faestermann, J. Friese, F. Heine, P. Kienle, E. Wefers, K. Zeitelhack, K. Beckert, B. Franzke, O. Klepper, C. Kozhuharov, G. Menzel, R. Moshammer, F. Nolden, H. Reich, B. Schlitt, M. Steck, T. Stöhlker, T. Winkler, and K. Takahashi. Observation of bound-state β^- decay of fully ionized ^{187}Re: ^{187}Re–^{187}Os cosmochronometry. *Phys. Rev. Lett.*, 77:5190 – 5193, Dec 1996.

[BLS13] F. Bosch, Y. A. Litvinov, and T. Stöhlker. Nuclear physics with unstable ions at storage rings. *Prog. Part. Nucl. Phys.*, 73(0):84 – 140, 2013.

[CAL14] CALIFA/R^{3}B Collaboration. Technical Report for the Design Construction and Commissioning of the CALIFA Endcap. Technical report, 2014.

[CPG+10] L. Chen, W. Plaß, H. Geissel, R. Knöbel, C. Kozhuharov, Y. Litvinov, Z. Patyk, C. Scheidenberger, K. Siegień-Iwaniuk, B. Sun, H. Weick, K. Beckert, P. Beller, F. Bosch, D. Boutin, L. Caceres, J. Carroll, D. Cullen, I. Cullen, B. Franzke, J. Gerl, M. Górska, G. Jones, A. Kishada, J. Kurcewicz, S. Litvinov, Z. Liu, S. Mandal, F. Montes, G. Münzenberg, F. Nolden, T. Ohtsubo, Z. Podolyák, R. Propri, S. Rigby, N. Saito, T. Saito, M. Shindo, M. Steck, P. Ugorowski, P. Walker, S. Williams, M. Winkler, H.-J. Wollersheim, and T. Yamaguchi. Discovery and investigation of heavy neutron-rich isotopes with time-resolved schottky spectrometry in the element range from thallium to actinium. *Phys. Lett. B*, 691(5):234 – 237, 2010.

[DWK16] G. D. Dracoulis, P. M. Walker, and F. G. Kondev. Review of metastable states in heavy nuclei. *Rep. Prog. Phys.*, 79(076301):1–46, 2016.

[G+92] H. Geissel et al. The GSI projectile fragment separator (FRS); a versatile magnetic system for relativistic heavy ions. *Nucl. Instrum. Meth. B*, 70:286 – 297, 1992.

[Gut01] H. H. Gutbrod. An international accelerator facility for beams of ions and antiprotons, Conceptual Design Report. Technical report, FAIR, 2001.

[JBB+92] M. Jung, F. Bosch, K. Beckert, H. Eickhoff, H. Folger, B. Franzke, A. Gruber, P. Kienle, O. Klepper, W. Koenig, C. Kozhuharov, R. Mann, R. Moshammer, F. Nolden, U. Schaaf, G. Soff, P. Spädtke, M. Steck, T. Stöhlker, and K. Sümmerer. First observation of bound-state β^- decay. *Phys. Rev. Lett.*, 69:2164 – 2167, Oct 1992.

[KAMF+14] N. Kurz, J. Adamczewski-Musch, J. Frühauf, J. Hoffmann, D. Beck, M. Kreider, C. Prados, S. Rauch, W. Terpstra, and M. Zweig. White Rabbit Applications for FAIR Experiments. *GSI Report*, 2014(1):380, 2014. dio:10.15120/GR-2014-1-FG-CS-09.

[KK03] O. Klepper and C. Kozhuharov. Particle detectors for beam diagnosis and for experiments with stable and radioactive ions in the storage-cooler ring ESR. *Nucl. Instrum. Meth. B*, 204(0):553 – 556, 2003.

[LB11] Y. A. Litvinov and F. Bosch. Beta decay of highly charged ions. *Rep. Prog. Phys.*, 74(1):016301, 2011.

[LBW+08] Y. A. Litvinov, F. Bosch, N. Winckler, D. Boutin, H. Essel, T. Faestermann, H. Geissel, S. Hess, P. Kienle, R. Knöbel, C. Kozhuharov, J. Kurcewicz, L. Maier, K. Beckert, P. Beller, C. Brandau, L. Chen, C. Dimopoulou, B. Fabian, A. Fragner, E. Haettner, M. Hausmann, S. Litvinov, M. Mazzocco, F. Montes, A. Musumarra, C. Nociforo, F. Nolden, W. Plaß, A. Prochazka, R. Reda, R. Reuschl, C. Scheidenberger, M. Steck, T. Stöhlker, S. Torilov, M. Trassinelli, B. Sun, H. Weick, and M. Winkler. Observation of non-exponential orbital electron capture decays of hydrogen-like ^{140}Pr and ^{142}Pm ions. *Phys. Lett. B*, 664(3):162 – 168, 2008.

[Mai07] L. W. Maier. *Speicherringexperiment zum gebundenen Beta-Zerfall vollstaendig ionisierter ^{207}Tl Kerne.* PhD thesis, Technische Universität München, Germany, 2007.

[MFK+01] L. Maier, T. Faestermann, P. Kienle, R. Schneider, A. Stolz, and W. E. A new detector system for measuring the bound state beta-decay of fully ionized ^{205}tl at the esr. *GSI Report 2000-1*, 1999(1):210, 2001.

[MHKO10] S. Minami, J. Hoffmann, N. Kurz, and W. Ott. Design and implementation of a data transfer protocol via optical fiber. *Real Time Conference (RT) IEEE-NPS*, 17:1 – 3, 2010. doi:10.1109/RTC.2010.5750447.

[NDB+16] M. Najafi, I. Dillmann, F. Bosch, T. Faestermann, B. Gao, R. Gernhäuser, C. Kozhuharov, S. Litvinov, Y. Litvinov, L. Maier, F. Nolden, U. Popp, M. Sanjari, U. Spillmann, M. Steck, T. Stöhlker, and H. Weick. Csi–silicon particle detector for heavy ions orbiting in storage rings (csisiphos). *Nuclear Instruments and Methods in Physics Research Section A: Accelerators, Spectrometers, Detectors and Associated Equipment*, 836:1 – 6, 2016.

[nnd] National Nuclear Data Center Brookhaven National Laboratory. http://www.nndc.bnl/gov/.

[Nov16] B. Novosibirsk. Technical Design Report for the collector ring, annex 1 v7.6.1. Technical report, BINP Novosibirsk, 2016.

[RCW+10] M. W. Reed, I. J. Cullen, P. M. Walker, Y. A. Litvinov, K. Blaum, F. Bosch, C. Brandau, J. J. Carroll, D. M. Cullen, A. Y. Deo, B. Detwiller, C. Dimopoulou, G. D. Dracoulis, F. Farinon, H. Geissel, E. Haettner, M. Heil, R. S. Kempley, R. Knöbel, C. Kozhuharov, J. Kurcewicz, N. Kuzminchuk, S. Litvinov, Z. Liu, R. Mao, C. Nociforo, F. Nolden, W. R. Plass, A. Prochazka, C. Scheidenberger, M. Steck, T. Stöhlker, B. Sun, T. P. D. Swan, G. Trees, H. Weick, N. Winckler, M. Winkler, P. J. Woods, and T. Yamaguchi. Discovery of highly excited long-lived isomers in neutron-rich hafnium and tantalum isotopes through direct mass measurements. *Phys. Rev. Lett.*, 105:172501, Oct 2010.

[SCL+13] D. Shubina, R. B. Cakirli, Y. A. Litvinov, K. Blaum, C. Brandau, F. Bosch, J. J. Carroll, R. F. Casten, D. M. Cullen, I. J. Cullen, A. Y. Deo, B. Detwiler, C. Dimopoulou, F. Farinon, H. Geissel, E. Haettner, M. Heil, R. S. Kempley, C. Kozhuharov, R. Knöbel, J. Kurcewicz, N. Kuzminchuk, S. A. Litvinov, Z. Liu, R. Mao, C. Nociforo, F. Nolden, Z. Patyk, W. R. Plass, A. Prochazka, M. W. Reed, M. S. Sanjari, C. Scheidenberger, M. Steck, T. Stöhlker, B. Sun, T. P. D. Swan, G. Trees, P. M. Walker, H. Weick, N. Winckler, M. Winkler, P. J. Woods, T. Yamaguchi, and C. Zhou. Schottky mass measurements of heavy neutron-rich nuclides in the element range $70 \leq Z \leq 79$ at the GSI Experimental Storage Ring. *Phys. Rev. C*, 88:024310, 2013.

[Wei] H. Weick. ATIMA website. https://web-docs.gsi.de/~weick/atima/.

[WGL+09] N. Winckler, H. Geissel, Y. Litvinov, K. Beckert, F. Bosch, D. Boutin, C. Brandau, L. Chen, C. Dimopoulou, H. Essel, B. Fabian, T. Faestermann, A. Fragner, E. Haettner, S. Hess, P. Kienle, R. Knöbel, C. Kozhuharov, S. Litvinov, M. Mazzocco, F. Montes, G. Münzenberg, C. Nociforo, F. Nolden, Z. Patyk, W. Plaß, A. Prochazka, R. Reda, R. Reuschl, C. Scheidenberger, M. Steck, T. Stöhlker, S. Y. Torilov, M. Trassinelli, B. Sun, H. Weick, and M. Winkler. Orbital electron capture decay of hydrogen- and helium-like ^{142}Pm ions. *Physics Letters B*, 679(1):36 – 40, 2009.

[WL06] P. M. Walker and Y. Litvinov. Technical Proposal for the ILIMA Project. Technical report, The ILIMA collaboration, 2006.

[WLG13] P. Walker, Y. A. Litvinov, and H. Geissel. The ILIMA project at FAIR. *Int. J Mass Spectrom.*, 349–350(0):247 – 254, 2013.